Impact of Microdialysis Probes on Vasculature and Dopamine in the Rat Striatum: a Combined Fluorescence and Voltammetric Study and The Design and Optimization of a Glutamate Sensor to be used under Hypoxic Conditions

by

Christina Marie Mitala

B.A Chemistry, Bucknell University, 2001

Submitted to the Graduate Faculty of

Arts and Sciences in partial fulfillment

of the requirements for the degree of

Doctor of Philosophy

University of Pittsburgh

2008

UNIVERSITY OF PITTSBURGH

School of Arts and Sciences

This dissertation was presented

by

Christina Marie Mitala

It was defended on

April 10, 2008

and approved by

Shigeru Amemiya, PhD, Assistant Professor, Chemistry Department

Stephane Petoud, PhD, Assistant Professor, Chemistry Department

Amy Wagner, MD, Faculty - Research, Physical Med & Rehabilitation Department

Dissertation Advisor: Adrian Michael, PhD, Associate Professor, Chemistry Department

Impact of Microdialysis Probes on Vasculature and Dopamine in the Rat Striatum: a Combined Fluorescence and Voltammetric Study and The Design and Optimization of a Glutamate Sensor to be used under Hypoxic Conditions

Christina M. Mitala, PhD

University of Pittsburgh, 2008

Measuring extracellular dopamine in the brain of living animals by means of microdialysis and/or voltammetry is a route towards understanding both normal brain function and pathology. Previous reports, however, suggest that the tissue response to implantation of devices may affect the outcome of the measurements. To address the source of the tissue response and its impact on striatal dopamine systems microdialysis probes were placed in the striatum of anesthetized rats. Images obtained by dual-label fluorescence microscopy show signs of ischemia, or reduced blood flow, and opening of the blood-brain barrier near the probe tracks. Opening of the blood-brain barrier was further examined by determining dialysate concentrations of carbi-DOPA, a drug that normally does not penetrate the brain. Although carbi-DOPA was recovered in brain dialysate, it did not alter dialysate dopamine levels or evoked dopamine release as measured by voltammetry near the probes. Microdialysis probes also significantly diminished the effect of intrastriatal infusion of kynurenate on extracellular dopamine levels as measured by voltammetry near the probes.

Glutamate is a very important neurotransmitter in the central nervous system. It is implicated in diseases such as schizophrenia, epilepsy, and stroke. Obtaining accurate information on glutamate concentrations is important in order to understand brain functioning. Glutamate is also of primary focus in terms of understanding the effects of hypoxia on the brain.

It is believed that the large release of glutamate in the absence of oxygen is what is causing the toxic effects of hypoxia. To date, sensors used to monitor glutamate required oxygen to be present. Here, the design and optimization of a glutamate sensor to be used under hypoxic conditions is presented.

TABLE OF CONTENTS

LIST OF FIGURES

PREFACE

I would like to take this opportunity to thank everyone who has made my years in graduate school successful. Above all, I would like to thank my advisor, Dr. Adrian Michael, for his support and guidance throughout the years. Dr. Michael is not only a good scientist and mentor, but also a personable person. Being able to just sit and talk about random things besides science made the working environment much more relaxing and pleasant. I appreciate the patience he has had with me; even when I was frustrated and convinced something wasn't going to work, he encouraged me to keep trying and to keep at it. I really appreciate all the valuable experiences and knowledge that I have gained while working under Dr. Michael. I would also like to thank my committee members; Drs. Shigeru Amemiya, Stephane Petoud, and Amy Wagner, and past and present members of the lab were vital to me in order to grow as a scientist.

Finally, I would like to thank my family. My parents have given me more support throughout graduate school than anyone could imagine, and believed in me when I had my doubts. I would like to thank my husband, Joe, who has been there for me the whole time. He listened to me practice talks so many times he could probably recite them and had patience with me when I felt completely overwhelmed. And last but not least, I would like to thank my sisters, brother, their significant others, and niece who also listened to me when I needed to vent, visited me when I just needed a friend nearby, and encouraged me along the way.

1.0   GAINING A BETTER UNDERSTANDING OF BRAIN CHEMISTRY: A CLOSER LOOK AT TECHNIQUE AND SENSOR DEVELOPMENT

1.1   IMPACT OF MICRODIALYSIS PROBES ON VASCULATURE AND DOPAMINE IN THE RAT STRIATUM: A COMBINED FLUORESCENCE AND VOLTAMMETRIC STUDY

1.1.1   Introduction

Measuring dopamine levels in the brain has been of interest for many years (Adams, 1990; Blaha, 1996; Garris et al., 1993; Garris and Wightman, 1994). The reason for the interest lies in the fact that dopamine plays a crucial role in motor control, cognition, and regulation of emotions. Deviations from "normal" levels of dopamine can also arise and are implicated in diseases such as substance abuse (Koob and Bloom, 1988), Parkinson's disease (Cookson, 2005), and attention-deficit hyperactivity disorder (Martinez-Leon, 2006). However, two of the main techniques used to measure dopamine, microdialysis and carbon fiber microelectrodes in conjunction with fast scan cyclic voltammetry, often produce results inconsistent with each other (Smith et al., 1992 and Borland et al., 2005). In fact, even carbon fiber microelectrode studies produce disagreeing results (Sabeti, et al, 2002 and Wu et al, 2001). It is crucial to understand these differences in order to fully understand what is occurring in the brain.

However, it must be noted that obtaining different "normal" levels of DA in the brain, 5 nM and 2.5 μM for microdialysis and voltammetry, respectively (Smith and Justice, 1994; and Borland et al., 2005), is not the only discrepancy. In fact, in terms of drug effects and kinetics, the results are "all over the map", so to speak.

1.1.2 Determining dopamine uptake and release

Regardless of technique, "normal" or basal levels of dopamine refers to the amount of dopamine in the extracellular space (ECS) of the brain. The amount of dopamine that can remain in the ECS is dependant upon two processes. One process is release and the other is uptake (Wightman and Zimmerman, 1990). Both methods agree on the uptake mechanism; dopamine is taken back up into the terminal through a dopamine transporter (DAT). However, how dopamine originally gets into the ECS is still under quite a bit of controversy, and thus has been under investigation for many years (Giorguieff et al, 1977; Leviel, 2001).

To date, there are two main theories on the modes of dopamine release; tonic and phasic release. Tonic release refers to the dopamine that is released from the dopamine transporter and phasic release refers to the dopamine that is released through a readily releasable pool that is stored within the neuron terminal. This readily releasable pool can be activated to bind with the neuron terminal, open, and release dopamine into the extracellular space upon receiving an action potential (Raiteri et al, 1979; Neher, 1998, Venton et al, 2006; and Leviel, 2001). Because phasic release is activated by neuron activation, it is also referred to as impulse-dependent release, whereas tonic release is often referred to as impulse-independent release.

The theory that there are two modes of dopamine release has been supported by experiments performed involving tetrodotoxin (TTX). TTX is a neurotoxin that blocks action

2

potentials in nerves. When TTX is administered, all phasic release of dopamine should be abolished (Giorguieff et al, 1977; Raiteri et al, 1979, and Desce et al, 1992). Due to the fact that dopamine release was not fully inhibited by TTX, it was concluded that some dopamine release is TTX-insensitive, or impulse-independent (Borland and Michael, 2004).   Microdialysis experiments challenged this notion of both impulse-independent and impulse-dependent release. Their claim was that all dopamine release was TTX-sensitive, or impulse dependent (Westerink et al, 1987; and Westerink and deVries, 1988). However, it must be noted, that there is one time in which microdialysis does detect TTX-insensitive dopamine; during the time frame directly after probe implantation. This time frame has also been attributed to when the tissue is healing after probe implantation, and therefore, microcialysis experiments will not commence until after a 24-hr healing period (Benveniste et al, 1987).

1.1.3   Conflicting results between and among methods

Since various methodologies disagree on how dopamine is released, it is conceivable that there would also be disagreement on the "normal" or basal dopamine concentration in the brain. As stated previously, Smith and Justice (1994) report basal dopamine levels of ~5 nM (microdialysis) while Borland and Michael (2004) report basal dopamine levels of ~2.5 μM (voltammetry). Although the exact cause of this discrepancy is still being debated, one possible explanation has to do with the amount of tissue damage created by implanting each device.

There are many other questions that remain unanswered. For instance, why does Wightman report a dopamine clearance rate order constant of ~16 s^{-1} (Jones et al, 1998) while Gerhardt reports a dopamine clearance rate order constant of 0.01 s^{-1} (Sabeti, et al, 2002), which is 1000 times slower? Why do microdialysis experiments indicate that nomifensine, a DA

3

uptake blocker, increases stimulated dopamine release while voltammetric experiments performed on carbon fibers indicate that nomifensine has a significantly less effect on stimulated dopamine release unless the fiber is placed directly next to a microdialysis probe (Borland et al, 2005)?

1.1.4   The dopamine gradient

To date, some of the differences between microdialysis and carbon fibers have largely been attributed to differences in the amount of tissue damage caused by implanting each device. Tissue damage created by implanting a microdialysis probe has been investigated by Clapp-Lilly et al (1999) and Zhou et al (2001). They concluded that there is an area of up to ~1.4 mm around a microdialysis probe in which damaged tissue was observed. This damaged tissue consisted of bloated axon terminals, distorted mitochondira, and fewer intact synapses. Peters et al (2004) reported only ~3 µm region around a carbon fiber in which damaged tissue occurred. This damaged tissue consisted primarily of darkened cytoplasm.

However, one of the drawbacks in trying to determine why discrepancies are occurring and what impact damaged tissue is having on detectable dopamine concentrations is that there is no simple way to perform an in vivo calibration (Tang et al, 2003). Of course, both can be calibrated in a beaker before and after an experiment, but that does not necessarily indicate what is occurring in the brain. For instance, a beaker is a static environment and there are no biochemical transports occurring. The closest that has been done to in vivo calibration is using these two methods side by side in the same tissue and comparing the results.

Borland et al, reports placing a carbon fiber electrode in three locations with respect to a microdialysis probe; adjacent, 200 µm away, and 1 mm away. At the electrode placed 1 mm

away, the concentration of dopamine detected after stimulation of the medial forebrain bundle was similar to that of a stand-alone electrode. At the electrode placed 200 μm away from the probe, a 90% decrease in stimulated dopamine as compared to a stand-alone electrode was reported, and at the electrode adjacent to the probe, neglibile dopamine was detected as compared to a stand-alone electrode. As stated previously, although this is not a direct calibration method, it is evident that in the tissue surrounding a microdialysis probe, there is a gradient of dopaminergic activity (Borland et al, 2005).

1.1.5 Brain vasculature

Because the distance separating blood vessels in the rat striatum (approximately 50 μm, Peters et al., 2004) is substantially less than the diameter of microdialysis probes, it is possible that blood vessels could be affected by probe implantation. Blood vessels, which carry red blood cells and are ultimately responsible for oxygen release, are in direct communication with neurons. In the case of dopamine, oxygen delivery to neurons through blood vessels is required to allow tyrosine hydroxylase to convert tyrosine to DOPA, which can then get converted to dopamine. This dopamine can be packaged and be available for release upon stimulation (Elsworth and Roth, 1997). A break-down in oxygen delivery would be detrimental in dopamine release.

Damaged blood vessels may also lead to the breakdown or increased permeability of the blood brain barrier. The blood brain barrier prevents certain species from entering the brain from the blood stream and a breakdown of the blood brain barrier could easily effect neurotransmitter release, uptake, and detection. Past research has revealed conflicting evidence on the status of the blood brain barrier. Groothuis et al (1998) reports that there is increased blood brain barrier permeability after probe implantation while Tossman et al., (1983) and Benveniste et al. (1984)

report no disruption of the blood brain barrier; however, there is little explanation about their results.

1.1.6   Objective of current study

It is the objective of this study to further investigate what the cause of the dopaminergic activity gradient is, and more broadly, to unravel the mystery creating discrepancies between and among analytical techniques.

In order to examine the blood vessels in the tissue sections containing probe tracks, I employed dual-label fluorescence microscopy. Blood vessels were labeled with dye-laden polystyrene nanobeads (100-nm diameter) delivered to the brain by transcardial perfusion. Tissue sections were also processed with anti-platelet endothelial cell adhesion molecule (antiPECAM), a marker for endothelial cells.

In order to gain a more clear understanding of the blood brain barrier permeability after probe implantation, I administered carbi-DOPA, a small molecule known to not be able to cross the blood brain barrier and inhibit dopamine synthesis. The dialysate was collected and analyzed for carbi-DOPA using HPLC-PFET. The effect of carbi-DOPA on stimulated dopamine was also investigated using carbon fiber microelectrodes and fast scan cyclic voltammetry.

1.2   ENZYME SENSORS TO BE USED UNDER HYPOXIC CONDITIONS

1.2.1   Hypoxia

Maintaining proper brain functioning relies on receiving adequate blood flow, such that oxygen and glucose are available when needed (Choi and Rothman, 1990). When oxygen levels become low, a state known as hypoxia arises (Gibson and Huang, 1992). Hypoxia is implicated in diseases such as stroke (Choi and Rothman, 1990) and Alzheimer's disease (Gibson and Huang, 1992).

Both in vitro and vivo studies have been performed to investigate the impact of hypoxia on brain function. Results indicate that hypoxia has a profound effect on neurotransmitter release. In particular, there is a decrease in acetylcholine release (Gibson and Huang, 1992) but an increase in dopamine (Gibson and Huang, 1992; Kuo et al, 1999) and glutamate release (Gibson and Huang, 1992), which leads to cognitive deficits in the former and postsynaptic damage in the latter two (Gibson and Huang, 1992).

1.2.2   Glutamate

Glutamate is a neurotransmitter that plays a crucial role in the central nervous system of mammals (Fonnum, 1984; Kulagina et al., 1999) and is implicated in diseases such as schizophrenia, Parkinson's disease, epilepsy, and stroke (Carlsson and Carlsson, 1990; Grace, 1991; Moghaddam, 1993; Kulagina et al., 1999). Obtaining accurate information on glutamate concentrations in the diseased and non-diseased laden brain is very important in not only understanding these diseases, but also in developing therapies to treat the diseases (Kulagina et

al., 1999). Glutamate is also of primary focus in terms of understanding the effects of hypoxia on the brain. It is believed that the large release of glutamate, and its implications on other cellular processes (Orset et al, 2006, Kuo et al, 1999), in the absence of oxygen is what is actually causing the toxic effects of hypoxia (Choi and Rothman, 1990).

1.2.3   Neurotoxic effects of glutamate

Glutamate, which is found in the excitatory presynaptic terminals in the brain, is required for neurotransmission, but can also be neurotoxic at greater concentrations (Olney and Sharpe, 1969; Olney, 1978; Choi and Rothman, 1990; Kashii et al, 1994). Under normal conditions, neuronal and glial uptake systems remove excess glutamate from the extracellular space before toxic levels are reached (Shousboe, 1981).   In cultured cortical neurons, exposure to 100 μM glutamate for five minutes resulted in a high number of destroyed neurons, suggesting that even a small amount of glutamate release can have a toxic effect on neurons (Choi et al, 1987).

The neurotoxic effects of glutamate, i.e., cytotoxicity, can also be accompanied by a toxic level of extracellular calcium influx (Choi and Rothman, 1990). One action of calcium influx is based on glutamate binding to a glutamate receptor on the NMDA (N-methyl-D-aspartate) complex. Once bound, the membrane channel can open and allow calcium to flow in. It must be noted, that a glutamate receptor NMDA antagonist can inhibit some of the neurotoxic effects of glutamate (Rothman, 1984; Choi et al, 1988).

Exposure to high concentrations of glutamate is also of concern due to its self-propagating nature. The initial injury causes a release of glutamate, but triggers further neuronal injury "mediated by the excessive release or leakage of endogenous glutamate stores" (Choi and

Rothman, 1990). However, Foster et al. (1988) report that administering a glutamate antagonist can lessen the detrimental effects of glutamate exposure (Foster et al, 1988).

1.2.4 Monitoring glutamate

Results obtained and reported above were obtained primarily in neuronal cultures (in vitro) or with a microdialysis probe in vivo. As presented earlier, voltammetric techniques at microelectrodes indicated that tissue up to 1 mm surrounding the microdialysis probe is damaged and displays characteristics of hypoxia. This tissue also displays a gradient of neurochemical activity; tissue proximal to the probe shows minimal activity while tissue distal to the probe shows greater activity (Borland et al., 2005). Therefore, it is imperative to develop a sensor with similar dimensions to the microelectrode to measure glutamate.

Electrochemical glutamate microsensors have been developed to monitor glutamate under normal conditions by employing a cross-linked redox polymer film containing enzymes. Glutamate oxidase is used to oxidize glutamate since it is not electroactive; a description of how the film works is described below. However, these microsensors need oxygen to function. Therefore, it is necessary to develop a technique to monitor glutamate in hypoxic environment.

1.2.5 Electrochemical detection of species using enzyme electrodes

Electrochemical detection of neurotransmitters and other species in the extracellular space of the brain has been performed by numerous research groups (Hu, Y., et al., 1994; Lowry, J.P., et al., 1998; Cui, J., et al., 2001, Kulagina, N.V., et al., 1999). Detection methods include using carbon fiber microelectrodes (Kulagina, N.V., et al., 1999; Garguilo, M.G. and Michael, A.C., 1996) as

9

well as Pt electrodes (Wang, J., et al., 1997; Hu, Y. and Wilson, G.S., 1997) in conjunction with an enzyme trapping redox macromolecule (Cui, J., et al., 2001; Garguilo, M.G. and Michael, A.C., 1996; Ohara, T.J., et al., 1994). These sensors "wire" enzymes to the electrode by using a cross-linked polymeric redox macromolecule composed of a poly(vinylpyridine) backbone derivitized with Os(bpy)$_2$Cl (Gregg and Heller, 1990; Heller, 1992; Kulagina et al., 1999; Kulagina and Michael, 2003). This polymeric redox macromolecule, often referred to as the hydrogel, allows substrates and their products to diffuse in and out of the gel since the enzymes are immobilized, and mediates the electron transfer between enzymes and electrode surface. This approach is particularly useful in detecting substrates that are not themselves electroactive.

1.2.6 Design of enzyme sensors to be used under hypoxic conditions

To date, enzyme sensors that employ redox hydrogels require oxygen to be present. However, in order to gain a better understanding of brain chemistry, it is important to be able to investigate species under hypoxic conditions as well. The approach taken here is to design a triple array band electrode in which the outer electrodes can generate a small amount of oxygen, creating a local environment that does contain oxygen, to drive the scheme contained within the hydrogel, and ultimately allow for the detection of species of interest at the center electrode.

The array band microelectrode, also referred to as an interdigitated array microelectrode, has been of interest recently. This type of microelectrode consists of an electrode being placed within a very small (μm) distance of another microelectrode (Iwasaki and Morita, 1995; Yang and Zhang, 2005), forming a microelectrode array. Any number of electrodes can be placed within this array and each one can have their own potential applied to it. The close proximity of the electrodes is very advantageous because it allows the diffusion layers of the electrodes to

overlap. This allows a species oxidized at one electrode (sometimes referred to as the generator electrode) to be able to diffuse to an adjacent electrode where it can be reduced (sometimes referred to as the collector electrode), or vice versa (Iwasaki and Morita, 1995; Yang and Zhang, 2005).

1.2.7 Glucose

Glucose is the primary source of energy for the brain. Glucose found in the extracellular space is brought there from the local cerebral blood flow, and changes in glucose demand are implicated in changes in blood flow. For example, an increase in blood flow is originally coupled to a decrease in glucose followed by a delayed increase (Fillenz and Lowry, 1998).

Glucose, as well as oxygen, regulates metabolism, angiogenesis, tumorigenesis and embryonic development. Although there has not been a significant amount of research performed on how the two interact, one study confirmed that there is communication between glucose and oxygen in the brain, and together play a role in physiological and pathophysiological brain processes (Kietzmann et al., 2002). Boutelle reports monitoring glucose-lactate ratios using microdialysis and an in-house built dual online assay after brain injury. Glucose-lactate ratios have been found to correlate with injury severity and have provided information about risks associated with treatment methods (Hopwood et al., 2005).

Again, it must be noted that most of the information on glucose levels have been obtained with microdialysis coupled with another analytical technique. The development of a sensor that is small, and can operate in real-time, in vivo, with high sensitivity and selectivity is necessary in order to understand brain function and dysfunction.

1.2.8 Objective of current study

The focus of the second half my research involves developing an enzyme sensor that can be used in the absence of oxygen. Such a sensor would be expected to be useful in probing neuroactivity at sensors containing oxidase enzymes in hypoxic conditions. To accomplish this, nanofabrication of a triple band Pt electrode in conjunction with photolithography was employed. The goal was to be able to generate oxygen at the outer two electrodes such that only minimal oxygen was produced, yet enough to drive the reaction scheme within the hydrogel. Before a functional electrode was made, there was much optimization involved in the design of the electrode and ratio of enzymes for the hydrogel. Although the primary goal is to develop a sensor for glutamate detection, developing a sensor to study glucose under hypoxic conditions is described here. Besides that fact that glucose in itself is interesting to study for the above mentioned reasons, glucose oxidase is also much cheaper and readily available than glutamate oxidase.

2.0   BRAIN VASCULATURE AFTER INJURY

2.1   ABSTRACT

Both microdialysis and voltammetry have been used to measure dopamine levels in the extracellular space in the brain of living animals. However, conditions exist under which these two dopamine-responsive techniques produce obviously different results even when used simultaneously in the same tissues. This creates uncertainty regarding the link between the measurements and dopaminergic physiology. Previously reports have suggested that these differences are related to the tissue response to probe implantation. The objective of the present report is to characterize the nature and extent of the tissue response. This report focuses attention on the impact of probe implantation on the microvasculature near the probe track. Inspection of blood vessels by fluorescence microscopy suggests that probe implantation causes an ischemic injury, or reduced blood flow, lasting throughout the 4 hr implant duration used in this study. Fluorescence microscopy in conjunction with carbi-DOPA microdialysis further suggests that probe implantation opens the blood brain barrier.

13

2.2   INTRODUCTION

Dopamine (DA) plays a crucial role in a variety of cognitive and motor functions and is implicated in substance abuse (Koob and Bloom, 1988), Parkinson's disease (Cookson, 2005), attention-deficit hyperactivity disorder (Martinez-Leon, 2006), stroke (Brannan et al., 1987), and traumatic brain injury (Ract et al., 2001). Measuring DA levels in the brain extracellular space (ECS) with in vivo microdialysis and/or voltammetry is a mainstay of investigations into both normal and pathological function of central DAergic systems (Kawagoe et al., 1993; Smith and Justice, 1994; DiChiara et al., 1996; Jones et al., 1998; Garris et al., 1999; Jones et al., 1999; Kulagina et al., 2001; Borland and Michael, 2004). On occasion, however, microdialysis and voltammetry produce different results (Bungay et al., 2003), even when they are performed simultaneously in individual animals (Lu et al., 1998; Yang et al., 1998; Borland et al., 2005). Understanding the origins of these differences is necessary to clarify the link between measured DA levels and physiology.

When microdialysis and voltammetry are performed simultaneously the difference in outcome depends on the spacing between the probe and the microelectrode. When the probe and microelectrode are in contact, e.g. glued to each other, the two measurements agree (Blaha, 1996; Yang et al., 1998) because the microelectrode measures dopamine in the fluid contacting the microdialysis probe. The voltammetric results change, however, if the spacing between the probe and the microelectrode is increased. When the spacing is about 1 mm, voltammetric results resemble those obtained in the absence of any probe, whereas intermediate results are

14

obtained at a spacing 200 μm (Yang et al., 1998; Borland et al., 2005). Thus, voltammetry reveals a gradient of DAergic function in the tissue surrounding the probes, the source of which is not yet understood.

Because the distance separating blood vessels in the rat striatum (approximately 50 μm, Peters et al., 2004) is substantially less than the diameter of microdialysis probes, we examined the impact of the probes on blood vessels. We employed dual-label fluorescence microscopy to image blood vessels in tissue sections containing probe tracks. Blood vessels were labeled with dye-laden polystyrene nanobeads (100-nm diameter) delivered to the brain by transcardial perfusion. Tissue sections were also processed with anti-platelet endothelial cell adhesion molecule (antiPECAM), a marker for endothelial cells.

Florescence microscopy revealed signs of ischemia and opening of the blood-brain barrier (BBB) near the probe tracks. Under normal conditions, the BBB restricts analytes from reaching the brain that do not belong there. It is important that the BBB remain intact, and restrict outside analytes, when monitoring brain functioning in order to gain a clearer understanding of how the brain works. We conducted further studies using carbi-DOPA as a probe of BBB permeability because it known to not be able to cross the BBB. Carbi-DOPA is useful in the treatment of Parkinson's disease because it acts in the periphery to inhibit the decarboxylation of l-DOPA. However, we found carbi-DOPA in striatal dialysates using microcolumn HPLC with PFET detection (Jung et al., 2006a; Jung et al., 2006b). Nevertheless, carbi-DOPA did not affect dialysate DA levels or evoked DA release as measured by voltammetry near the probes. We also assessed the effect of kynurenate on extracellular DA levels near microdialysis probes. In the absence of any microdialysis probe, kynurenate induces a tetrodotoxin-insensitive decrease in ECS DA from basal levels (Borland and Michael, 2004), a

15

finding that is difficult to rationalize with reports that basal dialysate DA is completely sensitive to TTX (Westerink and deVries, 1988; Westerink et al., 1989). We found, however, that the voltammetric response to kynurenate infusion is significantly diminished near the probes.

2.3   MATERIALS AND METHODS

2.3.1   Chemicals and solutions

2-methylbutane was obtained from Alfa Aesar (Ward Hill, MA). BSA, Triton-X 100, chloral hydrate, carbidopa, kynurenic acid and dopamine were used as received from Sigma (St. Louis, MO). Sucrose, BSA and chloral hydrate were dissolved in phosphate buffered saline (PBS: 155 mM NaCl, 100 mM phosphate, pH 7.4). Perfusion liquids include 2% paraformaldehyde (154mM sodium phosphate dibasic, 46mM sodium phosphate monobasic, and adjusted to pH 7.3 (7.2-7.4 is acceptable)) with NaOH or phosphoric acid; filtered (Iso-Disc TM filters, N-25-2 Nylon 25mm x 0.2μm, SUPELCO, Bellefonte, PA) added to 40g/L paraformaldehyde (Sigma, St. Louis, MO); final solution is 2% paraformaldehyde in 0.1M phosphate buffer and stored at 4°C) and a 0.1% solution of yellow-green fluorescent microspheres as received (0.1μm diameter, FluoSpheres® carboxylate-modified polystyrene microshpere suspensions (2% solids) in water plus 2mM sodium azide, Molecular Probes, Inc., Eugene, OR) in PBS . Sucrose was obtained from Fisher (Fisher Scientific, Pittsburgh, PA).   Probes were perfused with artificial cerebrospinal fluid (aCSF: 144 mM Na^+, 1.2 mM Ca^{2+}, 2.7 mM K^+, 152 mM Cl^-, 1.0 mM Mg^{2+}, and 2.0 M PO_4^{3-} adjusted to pH 7.4 with NaOH). Gelvatol was made as follows: 20 g polyvinyl alcohol (Sigma, St. Louis, MO) dissolved in 80 ml of 0.14 M NaCl solution buffered with 0.01 M KH_2PO_4-Na_2HPO_4 at pH 7.2 and stirred for 16h. 40 ml of glycerol (Sigma, St. Louis, MO) was added and stirred for another 16 h. In order to get rid of the undissolved particles, the

solution was centrifuged at 12000 rpm, afterwhich the supernatant was decanted and pH (around 7) was checked. 100 mg/ml DABCO (1,4-diazabicyclo [2.2.2] octane; Sigma, St. Louis, MO) was added. The solution was stored in an airtight bottle. All solutions were prepared with ultrapure water (NANOPure; Barnstead, Dubuque, IA).

2.3.2 Microdialysis probes

Vertical concentric microdialysis probes (220 μm o.d., 4 mm in length) were constructed with hollow fiber dialysis membrane (Spectra-Por RC Hollow Fiber, MWCO: 13,000, 160 μm i.d., Spectrum Laboratories, Inc., Rancho Dominguez, CA) and fused silica outlet lines (150 μm o.d., 75 μm i.d., Polymicro Technologies, Phoenix, AZ) as described elsewhere . All probes were perfused with aCSF at a rate of 0.586 μL/min.

2.3.3 Animals and surgical procedures

All procedures involving animals were carried out with the approval of the Institutional Animal Care and Use Committee of the University of Pittsburgh. Male Sprague-Dawley rats (Hilltop, Scottsdale, PA) (250-375g) were anesthetized with chloral hydrate (400 mg/kg i.p.) and wrapped in a homoeothermic blanket (EKEG Electronics, Vancouver, BC, Canada) to maintain a body temperature of $37^{o}C$. The rats were placed in a stereotaxic frame (David Kopf Instruments, Tujunga, CA) with the incisor bar 5 mm above the interaural line . Holes were drilled through the skull in the appropriate positions to expose the underlying dura and brain tissue. In the experiments requiring a reference electrode, the reference electrode made contact with the brain tissue via a modified salt bridge. The dura was removed with a scalpel to allow for placement of

the microelectrode and/or microdialysis probe into the brain tissue with minimal disruption to the surrounding blood vessels.

2.3.4   Microdialysis probe placement, tissue fixation, and processing

A microdialysis probe was slowly lowered over 30 min to a final position of 2.5 mm anterior to bregma, 2.5 mm lateral from midline and 7.0 mm below dura. The probe was perfused with aCSF at a rate of 0.586 µL/min for 4 hours. In one set of experiments, after the 4 hour implantation, the probe was removed after the rat underwent intracardial perfusion with 160cc of phosphate buffer solution (PBS), followed by 160cc of 2% paraformaldehyde and 50cc of 0.1% solution of yellow-green fluorescent microspheres. In the other set of experiments the probe was removed prior to the perfusion. Following the perfusion, the brain was removed, placed in 2% paraformaldehyde for 2 hours, and then placed in 30% sucrose overnight for cryo-protection.

The brain was removed from sucrose solution and frozen by dipping in liquid nitrogen-cooled 2-methylbutane. The frozen brain was transported to the microtome in dry ice or stored at -80°C until sliced. The frozen brain was mounted to the object holder with tissue freezing medium (Triangle Biomedical Sciences, Durham, NC) and Quick Freeze® (Electron Microscopy Sciences, Hatfield, PA). The brain was trimmed in 20-µm sections until the brain region of interest was reached. At this point, a 30-µm slice was cut and mounted onto a coverslide. Slides were stored at -20°C prior to antibody labeling.

2.3.5   Immunofluorescence protocol

On the day of labeling, the brain slices were removed from the freezer and rehydrated with two washes of 1xPBS (10x PBS, Fischer Scientific, Pittsburgh, PA and diluted with ultrapure water). The slices were treated with 0.1% Triton-X 100 in 1x PBS for 15 min to increase the permeability of the tissue . The slices were then washed three times with 0.5% bovine serum albumin (BSA), followed by a 45 min soak in 2% BSA. Finally, the slices were washed five more times with 0.5% BSA.

The prepared slices were soaked in 100uL of a 0.5% solution of as received primary antibody in 0.5% BSA (mouse anti-rat PECAM-1 [CD31]; Chemicon, Temecula, CA) for one hour. The slices were washed five times with 0.5% BSA, and then soaked for one hour in 100 µL of a 0.1% solution of as received secondary antibody in 0.5% BSA (goat anti-mouse IgG, CY3; Jackson Immunoresearch, West Grove, PA). The slices were washed five times with 0.5% BSA and five times with 1x PBS. The slices were soaked in Hoescht stain (diluted in de-ionized water for a final concentration of 1 mg/100 ml (Sigma, St. Louis, MO) for 30 s and washed three times with 1x PBS. The slices were covered with a gelvatol-treated coverslip and stored overnight in the dark at 4°C. The next day, the slices were imaged using a confocal microscope (Olympus Fluoview 1000 Confocal Microscope; Olympus, Melville, NY) or a fluorescence microscope (Olympus BX61; Olympus, Melville, NY).

2.3.6   Confocal microscopy

Confocal microscopy was used to obtain 3-D images of blood vessels. A multi-line argon laser was used to excite the yellow-green fluorescent microspheres at a wavelength of 488 nm, a green

helium-neon laser was used to excite the CY3 fluorochrome at a wavelength of 543 nm, and a diode laser was used to excite the Hoescht stain at a wavelength of 405 nm. All images were taken with a 20X objective lens. Confocal images were collected at 1.5 μm intervals in the z-axis. The images were analyzed with Metamorph/Fluor (Universal Imaging Corporation; Molecular Devices) and Adobe Photoshop (Adobe Systems Inc., San Jose, CA).

2.3.7 Fluorescence microscopy

Fluorescence microscopy was used to obtain the montage of images of the blood vessels that were double-labeled with the yellow-green fluorescent microspheres and PECAM. All images were collected with a 10X objective lens and the appropriate filter sets from Chroma Technology (Chroma, Rockingham, VT). Images were processed with Adobe Photoshop (Adobe Systems Inc., San Jose, CA).

2.3.8 HPLC analysis of carbi-DOPA and dopamine in microdialysate

In a separate set of animals, a microdialysis probe was lowered over 30 min into the striatum (2.5 mm anterior to bregma, 2.5 mm lateral from midline and 7.0 mm below dura). Microdialysate was sampled every 10 minutes beginning 2 hours after probe implantation. Carbi-DOPA (150 mg/kg i.p.) or vehicle (PBS) was administered 3 hours after probe implantation. Sampling continued at 10 minute intervals after drug administration. All samples were collected in microvials containing 0.65 μL of 1 M acetic acid.

The concentration of carbi-DOPA and dopamine in microdialysate samples were determined by means of high performance liquid chromatography with photoluminescence

following electron transfer detection (HPLC-PFET). The construction of the HPLC-PFET instrument was described in detail previously (Jung MC et al., 2006a). Separation of carbidopa in brain microdialysates was achieved using a reversed-phase, 100 μm i.d. capillary column at 1 μL/min flowrate. The mobile phase contained aqueous acetate-monochloroacetate buffer at pH 2.3, with 0.15 mM disodium EDTA and 13 mM sodium 1-octanesulfonate as an ion-interaction agent, mixed with 12.5% (v/v) acetonitrile. The separation required 8 min. The concentration detection limits of dopamine and carbidopa were 570 pM and 320 pM, respectively, with a 500 nL sample volume.

2.3.9 Voltammetric microelectrodes and techniques

Carbon fiber microcylinder electrodes were constructed as described previously (Borland and Michael, 2004). A single 7 μm diameter carbon fiber (Thornell Carbon Fiber, T300, Amoco Performance Products, Inc. Greenville, SC) was sealed with epoxy into a borosilicate glass capillary and trimmed to a length of 400 μm. The electrodes were pre-treated with 100 cycles of 0-2 V vs. Ag/AgCl triangular waveform delivered at 200 V/s. Dopamine and oxygen were detected by fast-scan cyclic voltammetry. The applied potential was held at 0 V vs. Ag/AgCl between scans. Dopamine was detected by linearly sweeping the potential to +1.0 V, then to -0.5 V, and back to the resting potential at a rate of 300 V/s, with the scans repeated every 100 ms. The dopamine oxidation signal was obtained by calculating the average current value between 0.6 and 0.8 V on the first sweep of each scan. Oxygen was detected by linearly sweeping from rest potential to -1.4 V and back to the resting potential at a rate of 300 V/s, with the scans repeated every 100 ms. The oxygen reduction signal was obtained by averaging the current between -1.1 V and -1.3 V on the first sweep of the scan. Background subtracted

voltammograms were obtained to confirm the presence of either dopamine or oxygen. The cyclic voltammograms were consistant with previously published reports and therefore are not shown here (Zimmerman and Wightman, 1991; Kennedy et al., 1992; Kulagina and Michael, 2003). Electrodes were calibrated before and after use in artificial cerebralspinal fluid containing known concentrations of dopamine.

2.3.10 Evoked oxygen response monitored at microelectrodes 220-250 μm from microdialysis probes

Evoked/stimulated oxygen responses were monitored 220-250 μm from an implanted microdialysis probe. The set-up of this experiment is described in detail elsewhere (Borland et al., 2005). A carbon fiber microelectrode was aligned at an angle to a microdialysis probe. The microelectrode was lowered into the striatum to a depth of approximately 4.5 mm below dura. A stainless steel bipolar stimulating electrode (MS303/1; Plastics One, Roanoke, VA) was lowered to the ipsilateral medial forebrain bundle (MFB: 2.2 mm posterior to bregma, 1.6 mm from midline, and initially 7.5 mm below dura). The MFB was stimulated with an optically isolated, constant current, biphasic square wave with a frequency of 60 Hz, a pulse width of 2 ms, a pulse height of 280 μA, and a train length of 10 s. The evoked dopamine response was monitored to confirm that the stimulating electrode had reached the MFB. Once a stable evoked dopamine response above 50 nA in amplitude was obtained, the potential waveform was changed to monitor evoked oxygen response. After a series of stable evoked oxygen responses were obtained, the microdialysis probe was slowly lowered over 30 min to a final position of 2.5 mm

anterior to bregma, 2.5 mm lateral from midline and 7.0 mm below dura. Electrical stimulation

commenced 2 hours after probe placement and continued at 20 min intervals.

2.4   RESULTS

2.4.1   Confocal microscopy and fluorescence microscopy of double-labeled blood vessels near microdialysis probes

Confocal and fluorescence microscopy of striatal slices from the brain hemisphere contralateral to probe implantation clearly reveals blood vessels labeled with fluorescent nanobeads (Fig 1a) and antiPECAM (Fig 1b). Overlaying the images yields excellent spatial correlation of the two labels (Fig 1c). Thus, Figure 2 demonstrates that the double labeling approach reliably images the intact brain microvasculature. The two labels are complementary since the nanobeads image perfusion flow and the antiPECAM images endothelium.

Microscopy of horizontal striatal slices obtained after four-hour probe implantations clearly reveals disruptions of the local vasculature near the probe tracks (Figs 2 and 3). Microscopy of these slices, oriented perpendicular to the longitudinal axis of the probes, clearly shows the probe tracks as dark, label-free spots approximately 300 μm in diameter. The probe tracks are surrounded by tissue that contains antiPECAM-labeled blood vessels totally devoid of fluorescent nanobeads. Furthermore, the probe tracks are surrounded by a halo of diffuse antiPECAM labeling. Although evident with all the probe tracks we examined, the dimensions of the halo and the nanobead-devoid region are variable. Moreover, the nanobead-devoid region is not centro-symmetric about the probe track itself (Figs 2 and 3).

25

Different images were obtained when transcardial perfusion was performed after removing probes from the tissue (Fig 4). The nanobead devoid region is almost eliminated except for a small region immediately adjacent to the probe track. Furthermore, the diffuse antiPECAM halo is absent. Together, these observations suggest that material causing a blockage of the blood vessels near the probe was dislodged when the probe was extracted. This enabled perfusion of the tissue near the probe track and access to that tissue by the nanobeads. A salient feature of these images, however, is the appearance of numerous nanobeads outside antiPECAM –labeled blood vessels (see arrows in Fig 4), showing the presence of leaking blood vessels adjacent to the probe.

a.   b.   c.
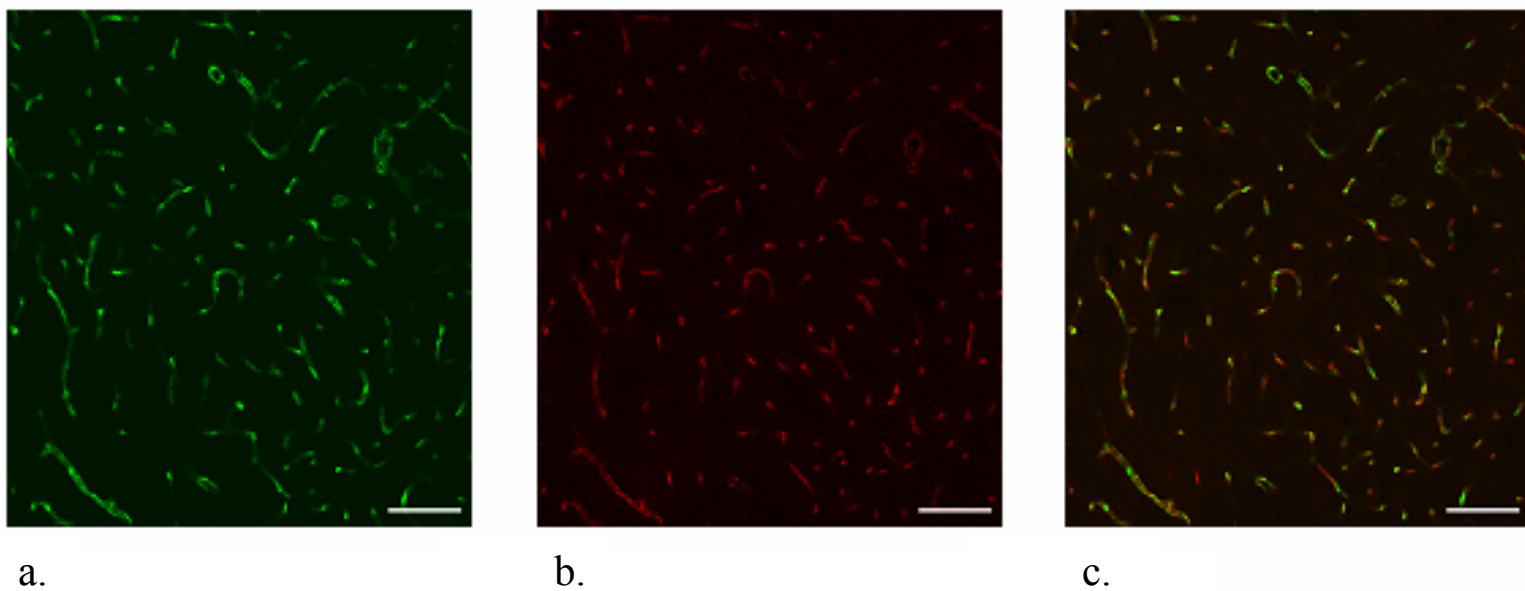
Figure 1: **Confocal microscopy of dual-labeled blood vessels in a horizontal section of the rat striatum contralateral to probe implantation (probe-free tissue). These images represent a Z-stack of optical sections taken at 1.5 mm intervals in the z-direction across a 30-μm thick brain slice. The scale bars represent 100 μm.**

a. Image of nanobeads fluorescence

b. Image of antiPECAM fluorescence.

c. Overlay of the images in a and b.
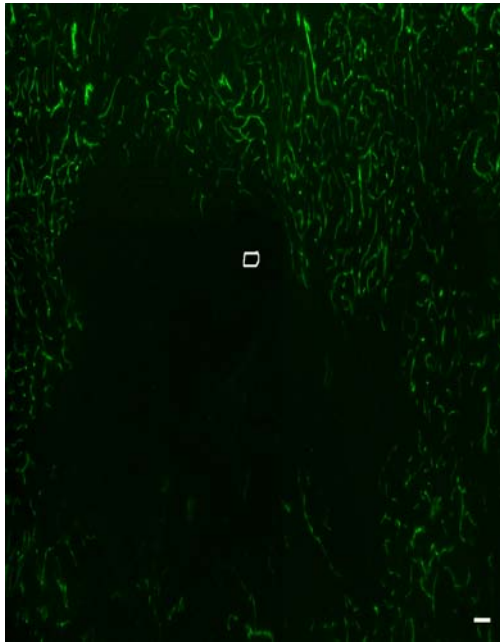
a.
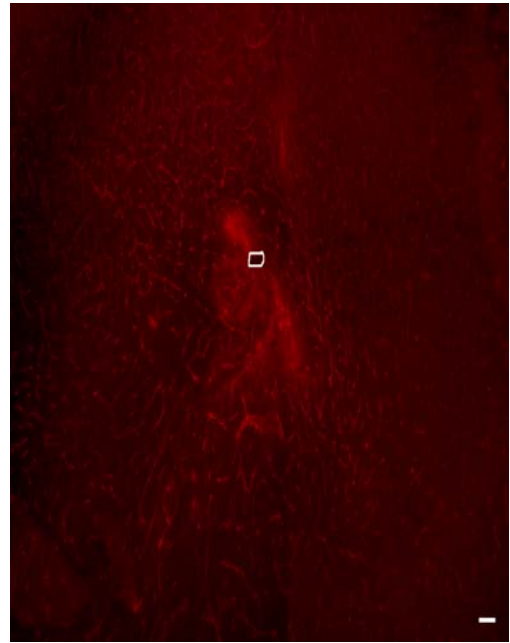
b.
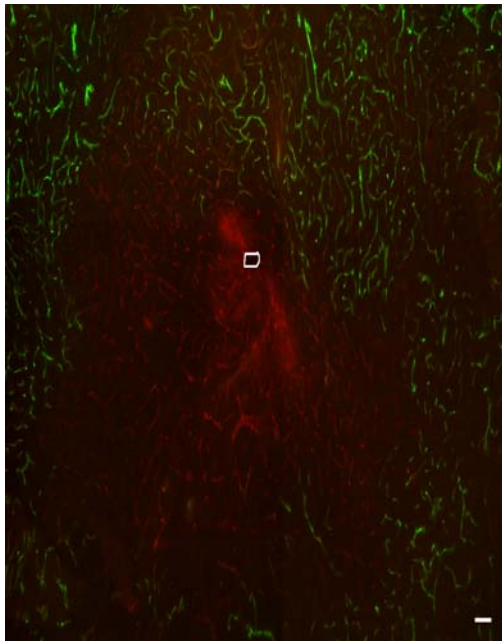
c.

Figure 2: Fluorescence microscopy of dual-labeled blood vessels in a 30-µm thick horizontal section of the rat striatum after a 4-hr probe implantation. The white circle represents the probe track. The scale bars represent 100 µm.

a. Image of nanobeads fluorescence.

b. Image of antiPECAM fluorescence.

c. Overlay of the images in a and b.
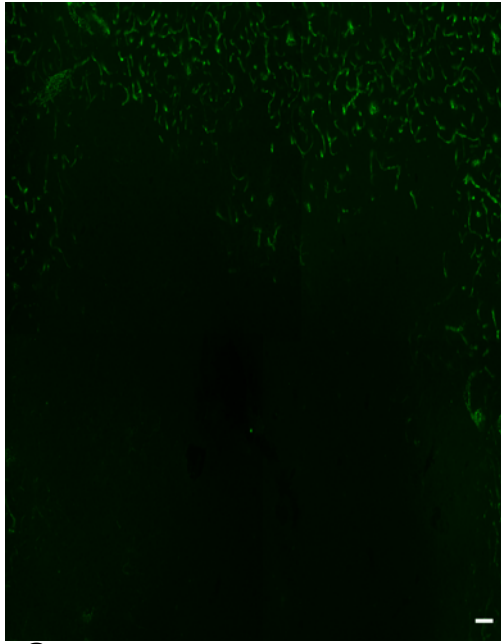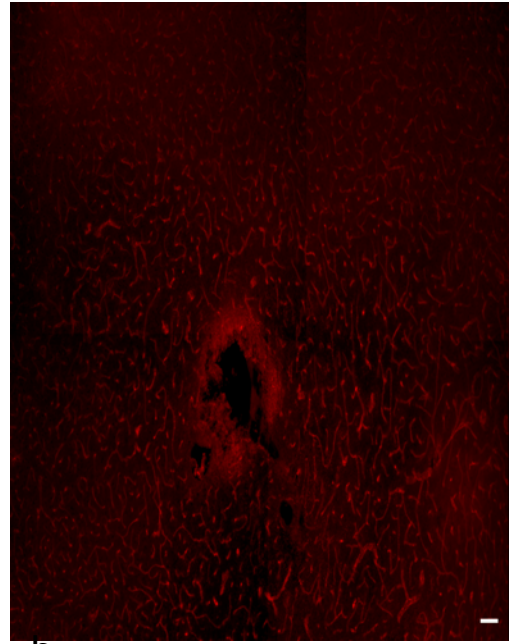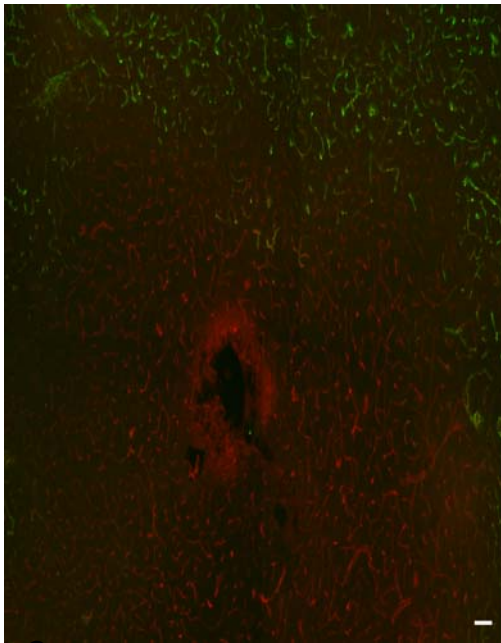
Figure 3: A second example of the images in Figure 2 from a different probe track in a different animal. The scale bars represent 100 μm.
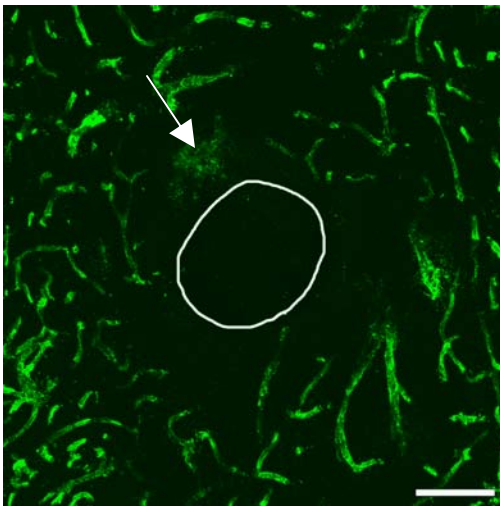
a.
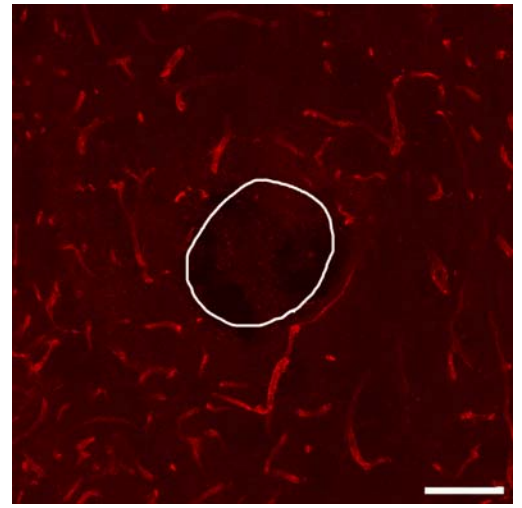
b.
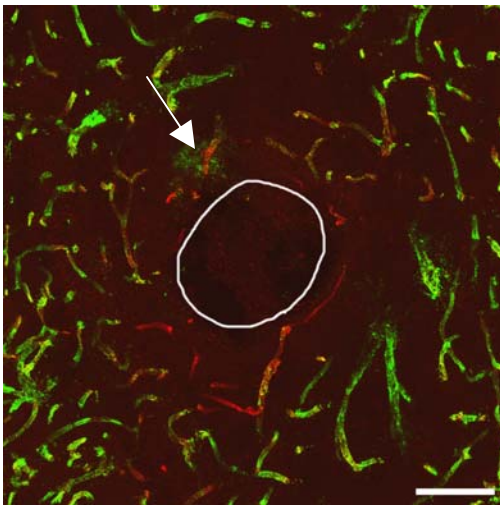
c.

Figure 4: **Fluorescence microscopy as in Figures 2 and 3 except that the microdialysis probe was extracted from the tissue prior to transcardial perfusion. Note the presence of nanobeads (green) outside blood vessels (white arrow). The white circle indicates the probe implantation track. The scale bars represent 100 μm.**

2.4.2   Analysis of rat brain microdialysate for carbi-DOPA and dopamine

Systemic administration of carbi-DOPA (150 mg/kg i.p.) increases carbi-DOPA levels in brain microdialysate samples (Fig 5). Calibration curves were constructed using standard solutions containing 0 – 100 nM carbi-DOPA and dopamine before analyzing each set of rat brain dialysates. Dialysate carbi-DOPA levels rose to approximately 80 nM after administration (blue squares; Fig 5).   Dialysate dopamine concentrations were unaffected (red circles; Fig 5).

n = 3 for dopamine and carbi-DOPA
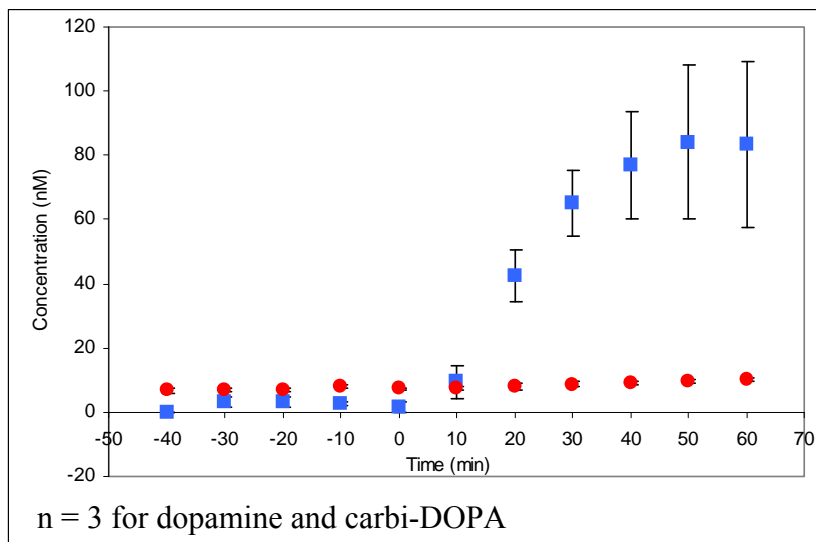
● dopamine

● carbi-DOPA

Figure 5: Systemic administration of carbi-DOPA (150 mg/kg i.p.) causes a significant increase in dialysate carbi-DOPA levels but has not effect on dialysate DA levels. (analysis by Moon Chul Jung) Notice the lack of decrease in dialysate dopamine levels after carbi-DOPA administration.

2.4.3   Voltammetric response of stimulated oxygen after probe implantation

Stimulation of the medial forebrain bundle resulted in oxygen release in the striatum as seen in an increase in current. Background subtracted voltammograms confirmed that the change in current was due to oxygen. The fact that current associated with evoked oxygen release after probe implantation did not return to baseline levels indicates that the cellular processes requiring oxygen are not taking place, thus oxygen is lingering in the extra cellular space (Fig 6).
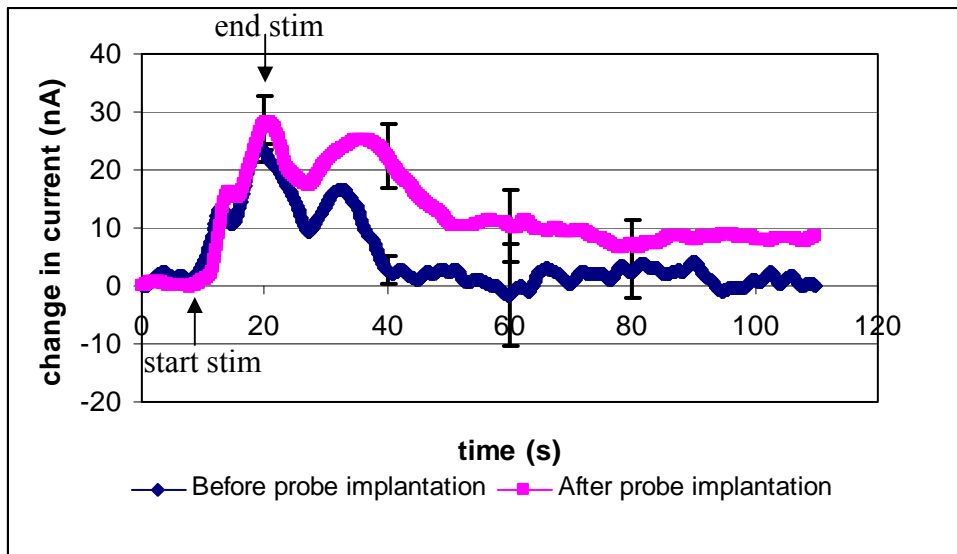
Figure 6: Change in current vs time plot of stimulated oxygen release. Notice the lingering oxygen current above pre-stim levels after probe implantation. The lingering oxygen suggests that cellular processes, including dopamine synthesis, are not utilizing the available oxygen, thus it is remaining in the extracellular space and is available for detection. The applied stimulus consisted of a 60 Hz pulse for ten seconds.

2.5   DISCUSSION

The findings of this study extend our previous voltammetric investigations (Lu et al., 1998; Peters and Michael, 1998; Yang et al., 1998; Qian et al., 1999; Yang et al., 2000; Borland et al., 2005) into the extent, nature, and neurochemical impact of the tissue response to the implantation of microdialysis probes.

Qualitative images obtained by fluorescence microscopy complement previous descriptions of the tissue response associated with microdialysis probe implantation (Clapp-Lilly et al., 1999). When transcardial perfusion was performed prior to removing the probes, blood vessels near the probe tracks were clearly labeled with antiPECAM but were devoid of fluorescent nanobeads (Figs 2 and 3). On the other hand, blood vessels in the contralateral striatum, i.e. probe-free tissue sections, were reliably double labeled. The absence of nanobeads in the vicinity of the tracks suggests that the probes trigger a localized ischemic event. A halo of antiPECAM labeling indicates the presence of endothelial cell debris at the probe track. These images confirm that vasculature disruption is a component of the acute (4-hr) tissue response to probe implantation.

The use of fluorescent nanobeads to determine patterns of blood flow is an established technology. Jasper and others employed this technology to examine blood flow in tissues as early as 1990 (Jasper et al., 1990; Van Oosterhout et al., 1998). Jasper introduced fluorescent nanobeads into the adrenals by injecting them via the left ventricle of the heart. The adrenals were subsequently excised, fixed in formalin, frozen, and cut into 80 μm sections. The

nanobeads were counted manually via fluorescence microscopy and a low count was attributed to low blood flow (Jasper et al., 1990). The carboxylate-modified fluorescent nanobeads that we employed are different from those used by Jasper et al. but are considered suitable for blood flow analysis because they do not have a high attraction for cells or vessel walls (Molecular Probes, 2004). Hence, we interpret the absence of nanobeads near probe tracks as a sign of impaired blood flow.

When transcardial perfusion was performed after removing the probes from the tissue, a different distribution of nanobeads was observed. The nanobeads were absent only from those blood vessels in closest proximity to the probe tracks (Fig 4). However, we also noticed nanobeads in interstitial spaces, i.e. outside blood vessels, near the tracks. The images suggest that the probe itself, which might compress adjacent tissues, was obstructing blood flow. Thus, removing the probe relieved the obstruction and improved tissue perfusion. In addition to obstructing vessels, however, the probe appears to tear them, allowing the nanobeads to leak into interstitial spaces when perfusion is performed after probe extraction (Fig 4). The antiPECAM halo in Figures 2 and 3 is consistent with the idea that vessels are torn and that endothelial cell debris is present at the probe track. The absence of the halo in Figure 4 suggests that the debris is washed out when perfusion is performed after probe extraction.

The appearance of nanobeads outside blood vessels (Fig 4) raises the possibility that the BBB is opened near the probe. On the other hand, opening the BBB might be inconsequential if blood flow to the probe is impaired. To investigate this issue, we administered carbi-DOPA, which normally does not penetrate the brain (Kaakkola et al., 1992). Consistent with a prior report (Kaakkola et al., 1992), we observed significant carbi-DOPA levels after systemic administration, suggesting that carbi-DOPA crossed the BBB.

We found it surprising that carbi-DOPA appeared in the dialysate, since florescence microscopy suggested impaired blood flow near the probes. However, the nanobeads are much larger than carbi-DOPA molecules. So, it appears to be the case that blood vessels near the probe are constricted in a fashion that prevents the flow of the larger objects, such as nanobeads and cells, but not the smaller carbi-DOPA molecules. Together, our findings suggest that although blood flow is impaired near the probes, perfusion of plasma or serum continues. Hence, small molecules, including nutrients and drugs such as carbi-DOPA, continue to reach the probes. The conclusion that small-molecule drugs have access to the probes is completely consistent with the many reports of drug-induced changes in dialysate DA levels.

Our conclusion that the BBB is opened by the implantation of a microdialysis probe contradicts some prior reports (Tossman et al., 1983; Benveniste et al., 1984). One of these prior reports, however (Tossman et al. 1983), makes only brief comment about the BBB. The other report (Benveniste et al. 1984) used a radiotracer method: we do not know specifically why our results are different except to say that there are several differences between the two studies (size of the probe, duration of the implant, etc.). However, in a later report these authors noted extravasated blood cells near probe tracks, a sign of probe-related injury (Benveniste, 1989). Furthermore, our suggestion that the perfusion of blood cells to probe tracks is inhibited while perfusion of serum or plasma continues is in line with an earlier report that the probes partially, but not completely, inhibit blood flow (Benveniste et al. 1987).

Despite the appearance of carbi-DOPA in dialysate following systemic administration, carbi-DOPA did not affect dialysate DA levels or evoked dopamine release as measured by voltammetry near the probe (Mitala et al., submitted). This stands in contrast to the well known ability of α-methyl-p-tyrosine, an inhibitor of tyrosine hydroxylase, to decrease dialysate DA

levels and the amplitude of evoked dopamine release (Stefano et al., 1976; Watanabe et al., 2005). The absence of a carbi-DOPA effect on evoked release is consistent with the idea that the drug crossed the BBB only in the immediate vicinity of the probe, i.e. only at those locations where we observed leaking vessels. If carbi-DOPA entered the brain only in these locations, it would have to diffuse from the track into surrounding tissue in order to affect evoked DA release. The diffusion process would lead to dilution, which would be exacerbated by the extraction of carbi-DOPA by the probe. Hence, at the site of the carbon fiber microelectrode, it is possible that the carbi-DOPA concentration was simply too low to affect evoked dopamine release. This explanation is consistent with the suggestion that the BBB is only opened very near the probe.

As shown here, small molecules, like carbi-DOPA can cross the blood brain barrier after probe implantation, but larger molecules, like red blood cells cannot. Since red blood cells are restricted, a localized hypoxic environment will occur. The question is now raised as to whether the terminals in that area are completely dead and whether the terminals can still respond to neurochemical stimuli. When the MFB is stimulated after probe implantation, an increase in current associated with oxygen is observed. This implies that the cells/terminals are not dead and can respond to neurochemical stimuli. It must be noted, that the current response remains above baseline levels for an extended period of time after stimulation, suggesting that since DA synthesis and other cellular processes are inhibited due to the lack of oxygen, the oxygen is lingering in the extracellular space (Fig 6).

Our report that the striatal extracellular space contains a pool of DA derived from TTX-insensitive release, presumably reverse transport (Borland and Michael, 2004), was surprising in light of the complete TTX-sensitivity of basal dialysate DA (Westerink and deVries, 1988;

Westerink et al., 1989). However, the implantation of a microdialysis probe significantly diminished the voltammetric response to intrastriatal infusion of kynurenate, raising the possibility that the absence of TTX-insensitive basal dialysate DA is part of the DAergic alteration associated with the tissue response to the probes (Mitala et al., submitted). To date, except in the case of amphetamine administration, TTX-insensitive dialysate DA has been attributed to tissue damage. For this reason, it is common to include in microdialysis procedures a 24 hr waiting period before samples are collected for analysis. The waiting period allows injury-derived extracellular dopamine to washout. While injury-derived DA release is very likely to be TTX-insensitive, it may not necessarily be the case that TTX-insensitive DA is exclusively derived from injury. Hence, the findings of the present study suggest that the role of TTX-insensitive DA release, even in the absence of amphetamines, deserves further examination.

Overall, this study contributes to a body of evidence for DAergic neurochemical alterations in the tissue surrounding microdialysis probes. Furthermore, our study suggests that these alterations are associated with ischemia and opening of the BBB. The observation of ischemia provides an explanation for the dramatic suppression of evoked DA release near the probes (~90%, this study and Borland et al., 2005). It is well known that DA terminals preferentially release newly synthesized DA. However, DA synthesis is an oxygen-dependent process (Takagi et al., 1995; Cooper et al., 1996; Bauer et al., 2000). So, probe-induced suppression of evoked DA release is attributable to decreased DA synthesis in the face of impaired oxygen delivery. Similar reasoning applies to the suppression of TTX-insensitive DA release (Mitala et al., submitted), since the TTX-insensitive response to kynurenate infusion is also dependent on newly synthesized DA (Kulagina et al., 2001).

Furthermore, the suggestion that DA synthesis is reduced in the face of impaired oxygen delivery is consistent with the large effects of the DA uptake inhibition on both evoked and non-evoked DA levels as measured by voltammetry near microdialysis probes (Borland et al., 2005). DA uptake inhibition mobilizes the DA reserve pool after synthesis inhibition (Miller and Shore, 1982; Ewing et al 1983; Venton et al., 2006). The large effect of DAT inhibition on voltammetric DA recordings near probes is consistent with this mechanism of action.

2.6   ACKNOWLDEGEMENTS

3.0   SELECTIVE DEPOSITION OF POLYMERS ONTO MICROELECTRODES

3.1   ABSTRACT

The ability to fabricate smaller and smaller devices, in particular electrodes, to monitor biological processes has advanced significantly in recent years. These smaller electrodes, termed microelectrodes and ultramicroelectrodes, display numerous advantages over larger electrodes, including faster response times and increased mass transport.   However, developing these devices is not the only hurdle to get over. Understanding the electrochemistry occurring at the microelectrodes is also crucial in their use. The microelectrodes that will be discussed in this work are triple array band microelectrodes. An advantage to having three electrodes on one chip is that different potentials can be applied to the three electrodes, and different polymers and/or hydrogels can be applied to each of the three electrodes in order to detect different analytes. Past research in our lab investigated the electrodeposition of poly-allylphenol onto one carbon fiber in a set of four carbon fiber microelectrodes arranged in a square fashion. Observation of these electrodes under a microscope revealed that although the electrodeposition of the polymer was onto only one electrode, the poly-allylphenol stretched across all four electrodes in a web-like manner. To the best of our knowledge, no one has explored how to control electrodeposition of polymers onto single electrodes in an array of electrodes. This paper carefully examines the

parameters necessary to specifically electrodeposit the polymer, 1,2-diaminobenzene, onto one electrode in an array.

3.2   INTRODUCTION

In recent years, the semiconductor industry has been putting forth great effort to develop microelectrodes for the electrochemical detection of small molecules (Wightman, 1981) and trace species (Iwasaki and Morita, 1995). Microelectrodes are advantageous over macroelectrodes primarily because of their small size and the properties associated with their small size. Some of these properties include being able to make chemical measurements in very small areas (brain) and measurements of time-independent currents. Because these currents are small, the electrode will not destroy the electrolyzed species and can be used in solutions with a high resistance (Wightman, 1981). One other very important property associated with microelectrodes is diffusion. Diffusion that occurs at a microelectrode is classified as spherical, meaning that a species can diffuse toward the electrode from all directions, as opposed to planar, which occurs at macroelectrodes, and means that a species can only diffuse toward the electrode head-on. Because the flux of the species toward a microelectrode can occur from all directions, the microelectrode provides a much higher degree of sensitivity than the macroelectrode (Iwasaki and Morita, 1995).

One type of microelectrode that has been of interest recently is an interdigitated array microelectrode. This type of microelectrode consists of an electrode being placed within a very small (micron) distance of another microelectrode (Iwasaki and Morita, 1995; Yang and Zhang, 2005), forming a microelectrode array. Any number of electrodes can be placed within this array

and each one can have their own potential applied to it. The close proximity of the electrodes is very advantageous because it allows the diffusion layers of the electrodes to overlap. This allows a species oxidized at one electrode (sometimes referred to as the generator electrode) to be able to diffuse to an adjacent electrode where it can be reduced (sometimes referred to as the collector electrode), or vice versa, numerous times (Iwasaki and Morita, 1995; Yang and Zhang, 2005).

There have been a few different techniques developed to fabricate these electrodes. One method involves depositing a metal between two insulator layers and then polishing/etching one of the sides to uncover the metal (Caston and McCarley, 2002; Lanyon and Arrigan, 2007). Another method involves using lithographic patterning and etching to evaporate the metal film (Lanyon and Arrigan, 2007; Morris et al., 1987). Although both methods prove effective, there are serious drawbacks to each. The first method relies on the deposition of the metal to determine the band thickness. Accurately determining the band thickness has proven to be difficult and the reproducibility has been low, thus this method has been more useful when only one band is being fabricated (Caston and McCarley, 2002; Lanyon and Arrigan, 2007). Although the second method produces reproducible structures, it is very expensive and requires many difficult processes to be carried out (Lanyon and Arrigan, 2007).

New techniques are still emerging, with the main driving force to be able to fabricate an electrode that has the same or similar dimensions to that of molecules. Of course, fabricating the electrode is not the only hurdle to get over. Once the electrodes are fabricated, the electrochemistry occurring at the electrode must be fully understood. Because of this, much of the recent research involving these electrodes lies in their optimization and characterization (Arrigan, 2004).

The use of these electrodes for application purposes is starting to come about, although the full potential of these electrodes is far from being reached (Arrigan, 2004). Burmeister, J.J., et al. (Burmeister et al., 2005), for example, reports using fabricated ceramic-based multisite microelectrodes to study L-lactate in brain tissue. His investigation was performed mainly in vitro, with preliminary data from in vivo. Other types of macroelectrode sensors are also being scaled down to microelectrode dimensions and fabricated as array electrodes instead of single electrodes. Array electrodes are particularly useful because different potentials can be applied to the different electrodes in the array and different electrodes can be coated with different layers to either detect or block various substances within the solution or environment (Arrigan, 2004).

One way in which a layer can be applied to a single electrode within an array is through electrodeposition. Electrodeposition occurs when a current is passed through an electrochemical cell from an outside source. Sasso, S.V., et al. (Sasso et al., 1990) reports electrodepositing 1,2-diaminobenzene (1,2-DAB) on a platinized, reticulated vitreous carbon electrode to act as an insulator to prevent interferences from species other than the analyte of interest and electrode fouling.

Poly-allylphenol has also been used for electrodeposition onto microelectrodes. In our hands, poly-allylphenol was used on carbon fiber microelectrodes. However, although the potential necessary to electrodeposit the poly-allylphenol was only applied to one carbon fiber microelectrode, the adjacent carbon fibers also became coated with the poly-allylphenol in a web-like manner. Because only the tip of the electrode was used for experiments, the webbing did not interfere with the experiment (Dressman et al., 2002). No one, to the best of our knowledge, has investigated how to control the electrodeposition of a substance onto only one

electrode in a series of electrodes, which would be instrumental in allowing for various analytes to be detected on different electrodes.

This paper investigates how to control the polymerization of 1,2-DAB onto one electrode in parallel with two other electrodes by controlling the scan time and number of potential sweep segments. In particular, after the electrodeposition of 1,2-DAB onto one electrode, a hydrogel, containing an osmium-based redox complex, was placed over all three electrodes. In order to ensure that the 1,2-DAB was insulating only the one electrode and not all three, the potential was swept between 0 and 600 mV; the potential in which osmium is oxidized and reduced. If the electrode was insulated, no redox peaks would be visible and if the 1,2-DAB was not acting like an insulator or was not present on the electrode, osmium redox peaks would be visible. Scan time and sweep segments were varied until the desired result was obtained.

3.3   MATERIALS AND METHODS

3.3.1   Chemicals and solutions

All reagents were used as received. Horseradish peroxidase (EC 1.11.1.7, type II, HRP), glucose oxidase (type II; from *Aspergillus niger*) and 1,2-diaminobenzene were obtained from Sigma (St. Louis, MO, USA). 4-(2-hydroxyethyl)-1-piperazineethanesulfonic acid (HEPES) and HEPES sodium salt were from Aldrich (Milwaukee, WI, USA). Poly(ethylene glycol 400 diglycidyl ether) (PEDGE) was from Polysciences Inc. (Warrington, PA, USA). 1,2-DAB was dissolved in phosphate buffered saline (PBS: 155 mM NaCl, 100 mM phosphate, pH 7.4). Ruthenium hexamine (III) chloride (RuHex) (Strem Chemicals, Newburyport, MA, USA) was

dissolved in 0.1 M KCL (EMD Chemicals, Inc, Gibbstwon, NJ, USA) for a final solution concentration of 10 mM. Chemicals for and the synthesis of the osmium redox hydrogel are as reported in Gregg, B.A. and Heller, A., (Gregg and Heller, 1990), and modified as reported in Mitala, J.J. and Michael, A.C. (Mitala and Michael, 2006),. All solutions were prepared with ultrapure water (NANOPure; Barnstead, Dubuque, IA).

3.3.2 Hydrogel films

The redox polymer (4 mg/mL, 20 uL) and cross-linker (PEDGE, 3 mg/mL, 16 uL) were dissolved in nano-pure DI water (Nanopure, Barstead, Dubuque, IA). HRP (3 mg/mL, 10 uL) and glucose oxidase (2 mg/mL, 10 uL) were dissolved in HEPES buffer (pH 8.00) prepared by the addition of HEPES sodium salt to a 10 mM solution of the acid.

3.3.3 Fabrication of array electrodes

Standard 3-in. silicon wafers were used as substrates. The wafer tops were insulated with silicon dioxide, followed by a layer of titanium and platinum. Titanium was used in order to promote adhesion between the silicon dioxide and platinum. These wafers were purchased from Silicon Quest International, Santa Clara, CA, USA. Photoresist and HMDS were deposited onto the wafer by spin coating (CEE 100CB Spinner/Hotplate). The resist was patterned using UV radiation (Karl Suss MA6 Backside Aligner) through a photomask (Penn State, State College, PA, USA) with the electrode pattern. The wafer was baked for one minute on a 100° C hotplate followed by washing away the resist on the exposed areas of the wafer with a resist developing bath. The wafer was baked for ten minutes in a 120° C oven before etching the Ti/Pt by ion

milling. The wafers were O_2 plasma cleaned (Technics Plasma Deposition System) before the insulating layer was applied. This removes any remaining photoresist. The wafers were baked on a 200°C hotplate for twenty minutes to ensure that all moisture was removed. The insulating layer, SU8, was applied using a spin plate (Solitec Photoresist Spinner) afterwhich the wafer was soft baked (65° up to 105° C and held there for ten minutes, and then slowly cooled). The insulating layer was patterned using UV radiation (Karl Suss MA56 Contact Aligner) through a second mask. The wafer was soft baked as stated above. The unexposed area on the wafer were rinsed away with developer, rinsed with IPA and dried with nitrogen. Again, the wafers were oxygen plasma cleaned to descum and hard baked in a 120° C oven for a few hours. The electrodes were diced with a Kulicke and Soffa 780-6 Dicing Saw. Fig 7.

100 um
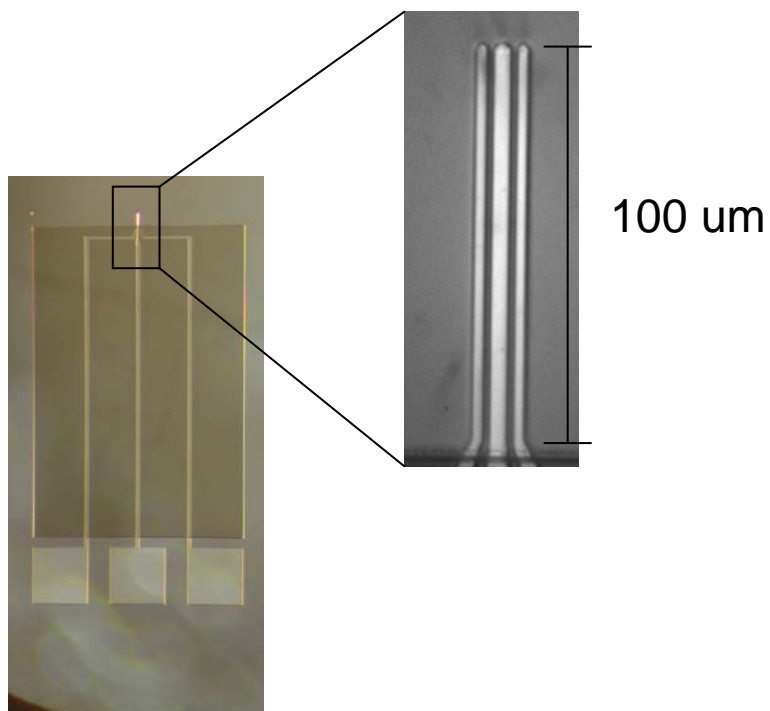
Figure 7 Array band platinum electrode. The only exposed platinum are the tip and contact pads. Insert is a close up of the tip.

3.3.4   Electrical connections to electrodes

Individual electrode chips were cleaned by sonicating (Branson, Danbury, CT, USA) in acetone (EMD Chemicals, Inc, Gibbstwon, NJ, USA) for fifteen minutes, rinsed with IPA (EMD Chemicals, Inc, Gibbstwon, NJ, USA), and dried with nitrogen (Valley National Gas, West Mifflin, PA, USA). Each chip was glued (5 – Min Epoxy, ITW Devcon, Danvers, MA, USA to a microscope slide (Fisher, Pittsburgh, PA) and oxygen plasma cleaned (Harrick Plasma Cleaner PDC-3XG, Ithaca, NY, USA) for five minutes, in house. Individual copper wires (Goodfellow, England) were placed such that one end rested on a single contact pad. Once all three wires were in place, the wires were epoxied to the slide. With silver paint, connections were made between the contact pad and wire. The electrodes were allowed to dry overnight.

3.3.5   Electrochemical techniques and hydrogel application

Cyclic voltammetry (Keithly Instruments, Cleveland, OH, USA), was performed to electrodeposit the 1,2-DAB onto a single electrode in the array. The potential was swept from -0.5 V to 1.0 V and back to -0.5 V vs Ag/AgCl reference electrode in a 3 mM 1,2-DAB solution. The electrodes were rinsed following electrodeposition. The number of sweeps varied from experiment to experiment.

In the first set of experiments, the potential was scanned until two successive scans produced overlapping cyclic voltammograms. In the second set of experiments, the potential was only scanned one time in the positive and negative direction. The third set of experiments employed fast scan cyclic voltammetry to electrodeposit the 1,2-DAB. Here, the

potential was swept from -0.5 V to 1.0 V and back to -0.5 V vs Ag/AgCl reference electrode in a 3 mM 1,2-DAB solution at a rate of 100V/s with a scan interval of 100 ms, and duration of 300 s. In the final set of experiments, fast scan cyclic voltammetry was used as stated above, except with a scan rate of 300 V/s, scan interval of 100 ms, and duration of 180 s. Scan rate and time were originally chosen by trial and error and were later adjusted based on results from previous experminets.

In the first three sets of experiments, 2 μL of the redox hydrogel was applied to all three electrodes after the electrodeposition. The electrodes were placed in a 37° C oven for one hour. After the allotted amount of time, the electrodes were placed in a beaker of PBS. The potential was swept from 0.0 V to 0.6 V or 1.0 V and back to 0.0 V in order to test whether osmium could be detected at each individual electrode surface.

In the final set of experiments, bare electrodes were placed in 10 mM RuHex. The potential was swept from -0.2 V to 0.7 V and back to -0.2 V using cyclic voltammetry to produce a "before electrodeposition" cyclic voltammogram. 1,2-DAB was electrodeposited onto the middle electrode as described previously for the final set of experiments. The electrode was rinsed and placed back in the RuHex solution. An "after electrodeposition" cyclic voltammogram was obtained in the same manner as the "before electrodeposition" cyclic voltammogram.

3.4   RESULTS

3.4.1   Full electrodeposition of 1,2-DAB on left-most electrode until two scans overlap and hydrogel application

The application of the potential between -0.5 V and 1.0 V and back to -0.5 V revealed a decreasing oxidation peak with each successive scan on the left most electrode.   Scans were continued until two scans overlapped.   In the plot shown here, the potential was scanned six times before two successive scans overlapped. Fig 8. Sweeping the potential from 0 to 600 mV after hydrogel application did not result in osmium detection at the middle/adjacent electrode. Fig 9.
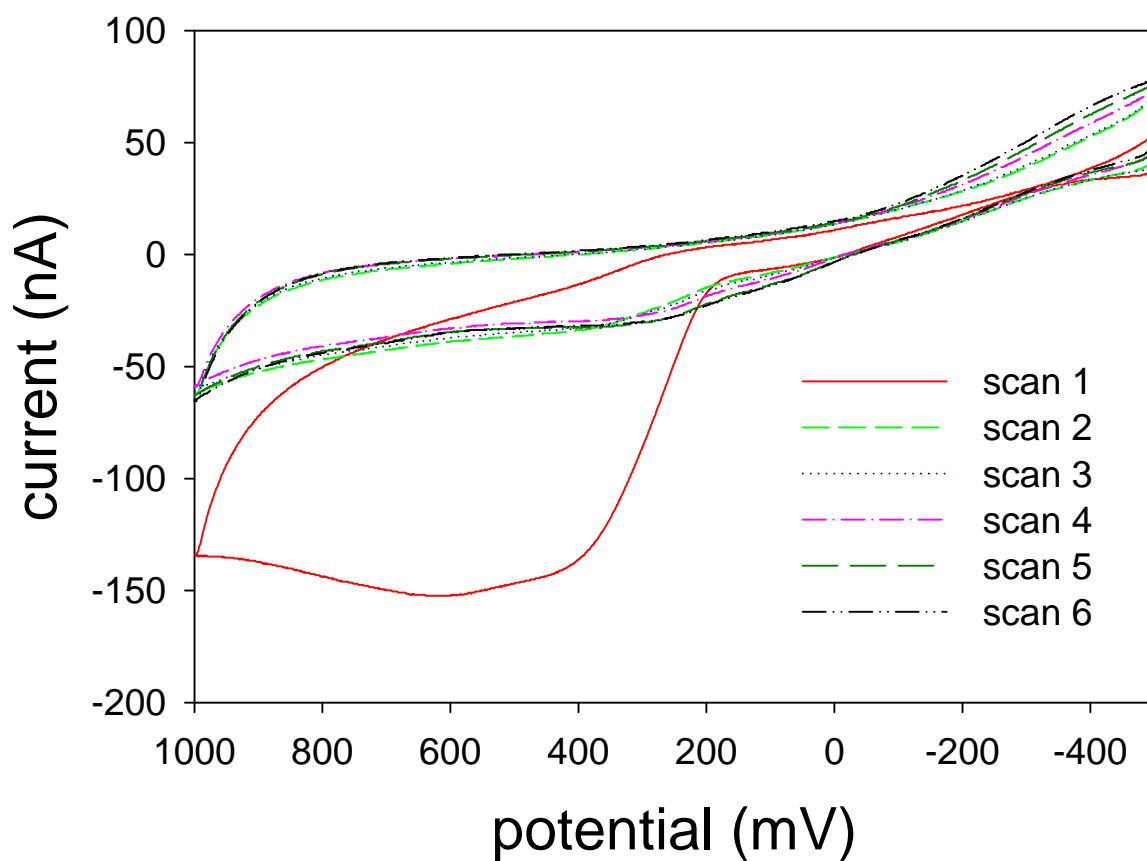
Figure 8: Electrodeposition of 1,2 – DAB on one of the platinum electrodes. Oxidation peak decreases with scan number and indicative of the polymeric film coating the electrode. As the film coats the electrode, less 1,2-DAB can reach the surface for oxidation.
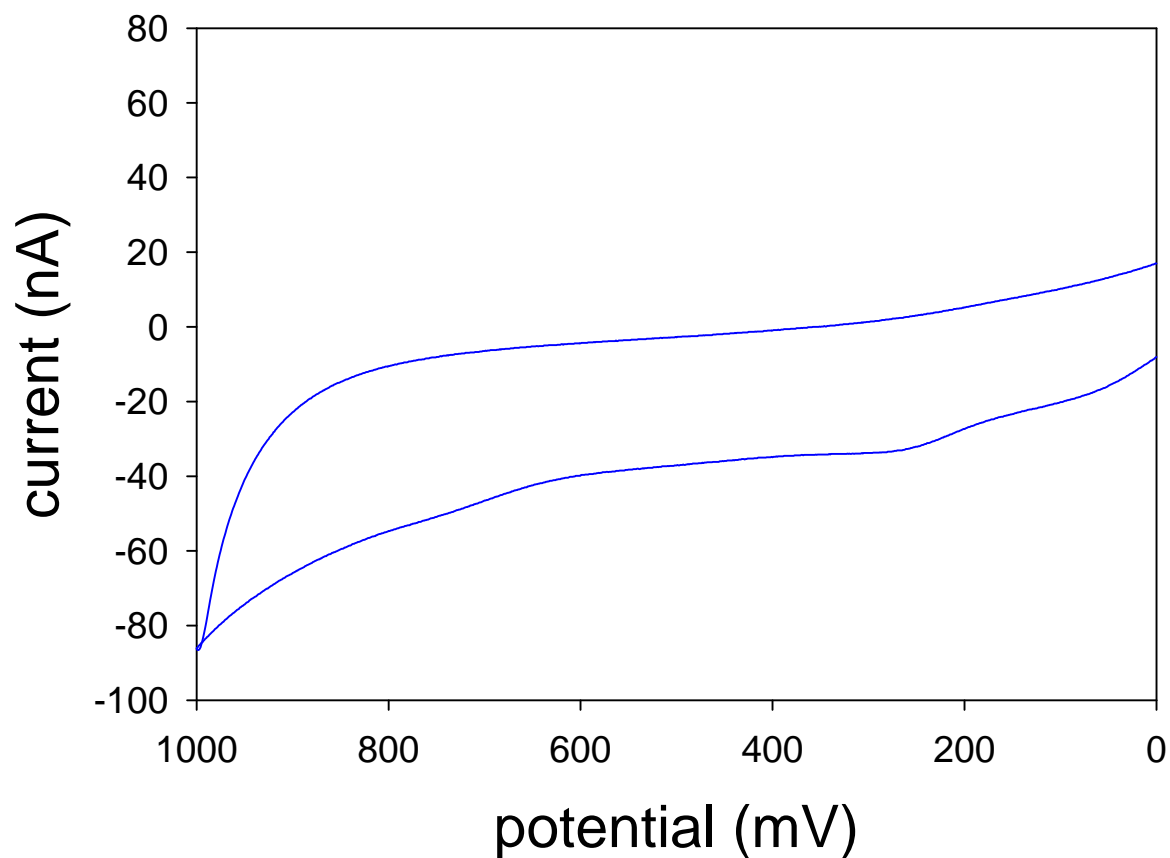
Figure 9: Middle electrode after electrodeposition of 1,2 – DAB on an adjacent electrode. The redox hydrogel has been applied, yet no osmium redox peaks are visible. This implies that the 1,2-DAB that should have been deposited only on the adjacent electrode somehow got deposited on the neighboring electrode and is preventing the osmium in the hydrogel from being detected.

3.4.2 Minimized electrodeposition on left-most electrode plus hydrogel application

One potential sweep from -0.5 V to 1.0 V to -0.5 V was applied to the left-most electrode in order to electrodeposit the 1,2-DAB. Sweeping the potential after hydrogel application resulted in small redox peaks on the middle electrode and slightly larger redox peaks on the right most electrode. Fig 10.
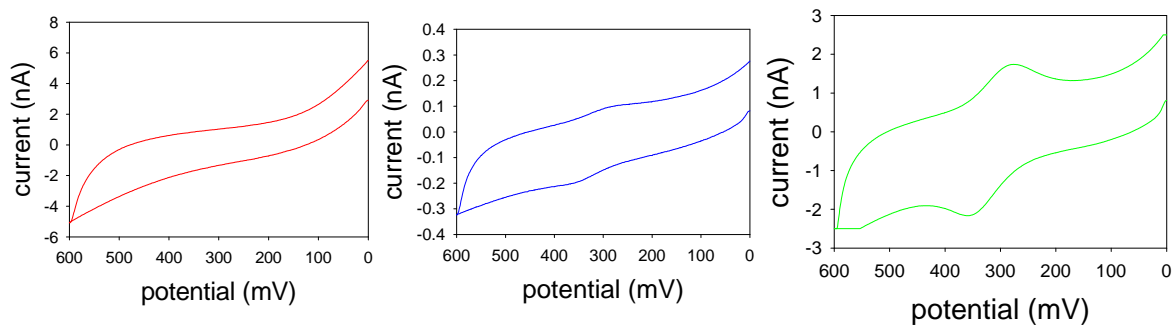
Figure 10: **Fewer sweep segments for the electrodeposition of the 1,2 – DAB onto the left electrode. Hydrogel has been applied and osmium peaks are visible at the middle and right electrode although the sensistivity is not equal. Left electrode is shown in the left-most plot, middle electrode in the center plot, and right electrode in the plot on the right.**

3.4.3 Fast scan cyclic voltammetry for electrodeposition plus hydrogel application

The potential was swept from -0.5 V to 1.0 V and back to -0.5 V vs Ag/AgCl reference electrode in a 3 mM 1,2-DAB solution at a rate of 100V/s with a scan interval of 100 ms, and duration of 300 s. Sweeping the potential after hydrogel application resulted in no osmium peaks seen on the electrode that had 1,2-DAB on it. The middle and right electrode both showed osmium redox peaks that were similar in amplitude. Fig 11. When the same experiment was performed, except for that the middle electrode was electrodeposited with the 1,2-DAB instead of the left electrode, the right and left electrodes displayed cyclic voltammograms with osmium redox peaks of similar amplitude, while the middle electrode did not produce a cyclic voltammogram with osmium redox peaks. Fig 12.
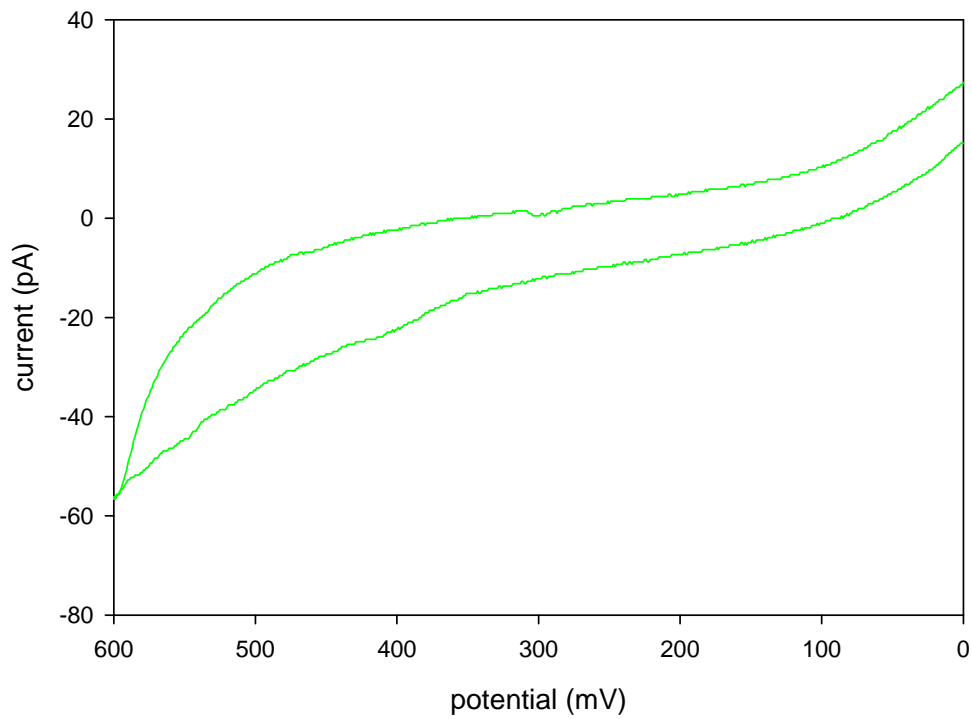
left - has 1,2-DAB and hydrogel
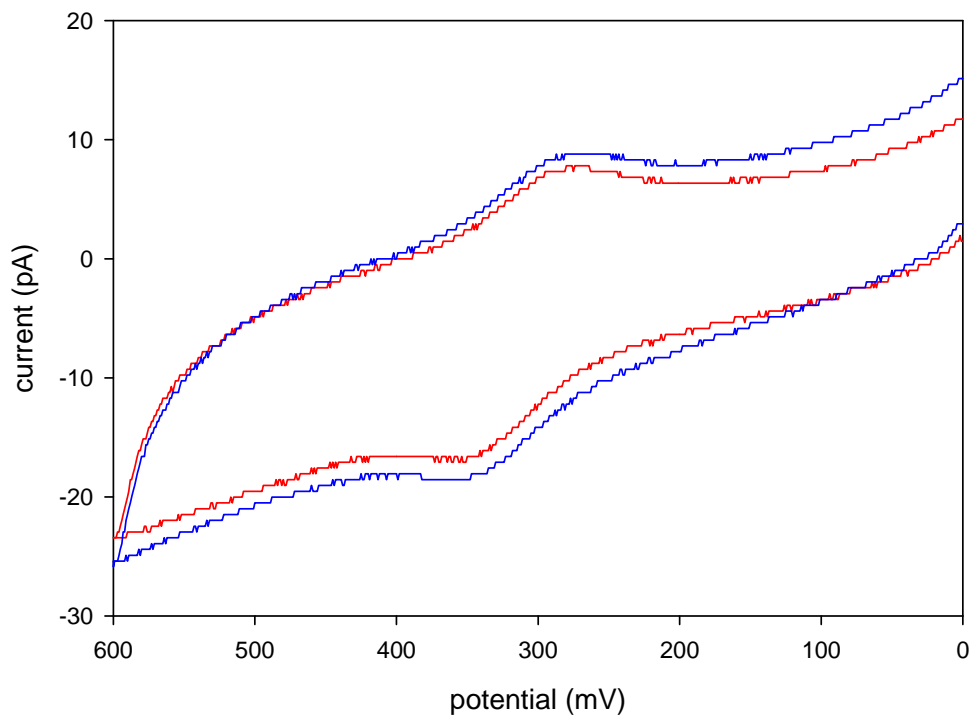
middle - only hydrogel
right - only hydrogel

Figure 11: Electrodeposition of 1,2 – DAB onto the left electrode using fast scan cyclic voltammetry. Hydrogel has been applied and osmium redox peaks on the middle and right electrode are visible and have similar sensitivity.
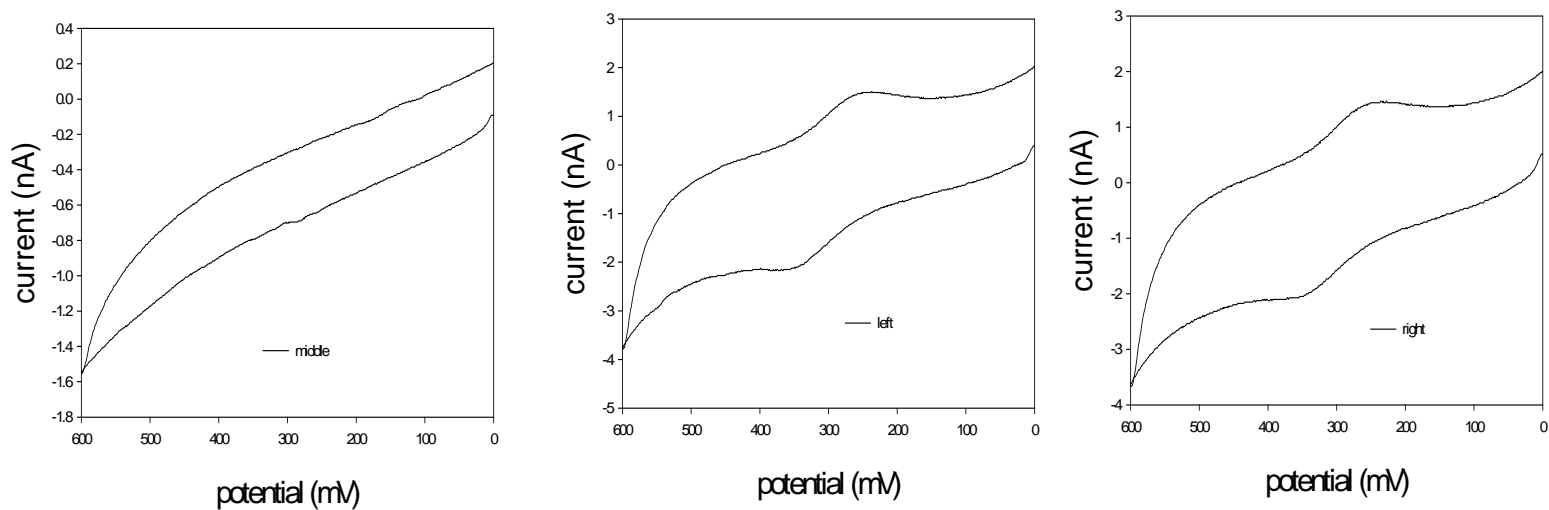
Figure 12: Electrodeposition of 1,2 – DAB onto the middle electrode using fast scan cyclic voltammetry. Hydrogel has been applied and osmium redox peaks on the left and right electrode are visible and have similar sensitivity.

3.4.4   RuHex and fast scan cyclic voltammetry to monitor electrodeposition

Sweeping the potential from -0.2 V to 0.7 V and back to -0.2 V in RuHex before and after the 1,2-DAB electrodeposition on the middle electrode, produced cyclic voltammograms of the outer electrodes that were virtually the same. This suggests that although the current is small, the effect of electrodeposition on an adjacent electrode is not effecting the sensitivity of that electrode. The middle electrode could no longer detect the reduction of RuHex. Fig 13.
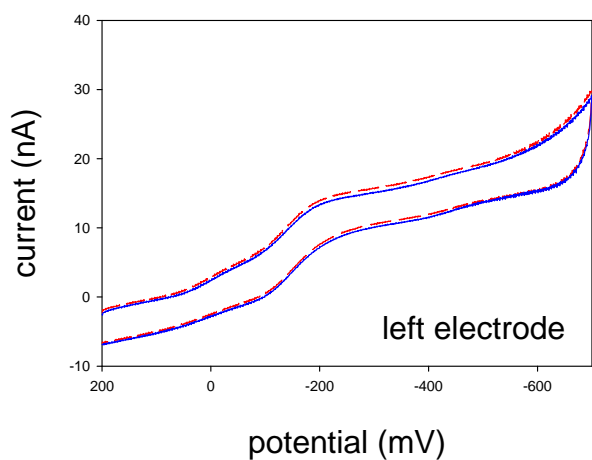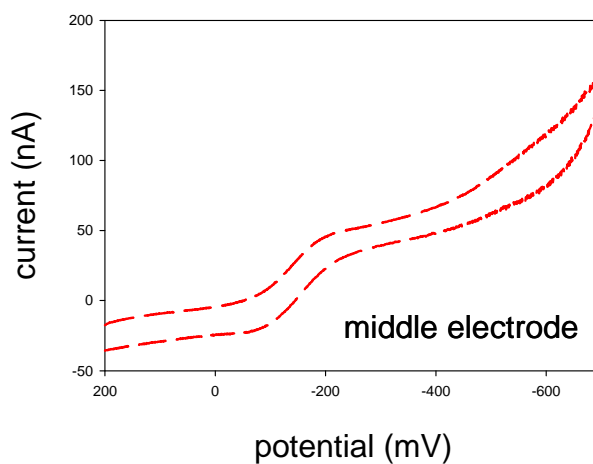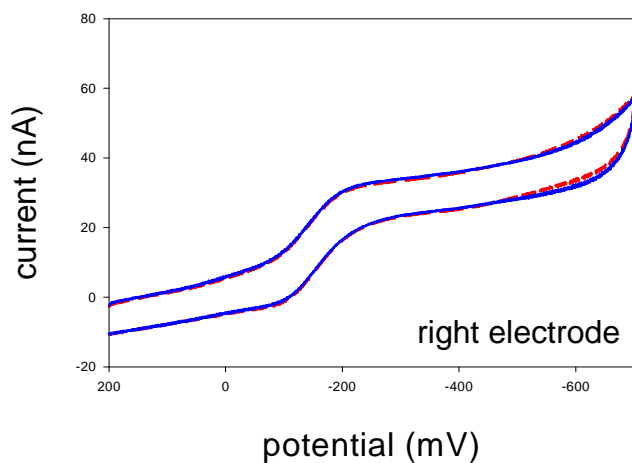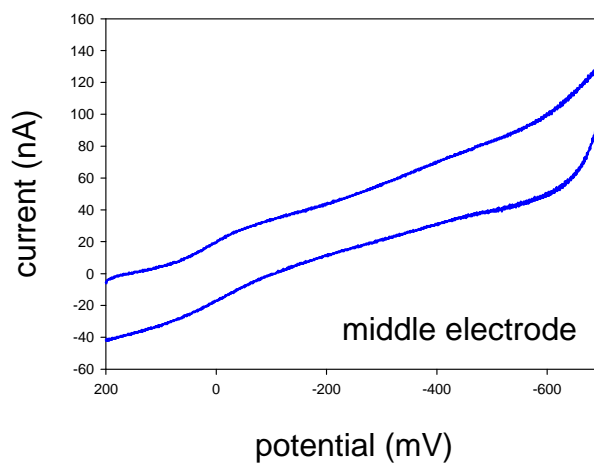
Figure 13: Before and after cyclic voltammograms of the left, middle, and right electrode in 10 mM RuHex. Between the before and after cyclic voltammograms, 1,2 − DAB was electrodeposited onto the middle electrode using fast scan cyclic voltammetry.

3.5   DISCUSSION

Heineman reports that 1,2-DAB can be electrodeposited onto an electrode by the following technique. The potential is swept from 0.0 to +0.8 V vs SCE reference electrode, producing a cyclic voltammogram displaying a large irreversible oxidative current with a peak current at +0.51V vs. SCE. Successive scans result in a drastically reduced peak current until scans started to overlap, representing no flow of current and the electrode being fully coated with the insulating layer (Heineman et al., 1980).

We were able to repeat that procedure and obtain the same results by applying the potential to one of the electrodes in the array. The cyclic voltammograms obtained resulted in a decrease in oxidative current with the final two sweeps resulting in direct overlap, indicating the electrode is coated with a thin layer of the polymer. The redox hydrogel was applied to all three electrodes, after which an applied potential sweep between 0 and 1000 mV was applied to the middle (adjacent) electrode. The purpose of this is to verify the connection between the osmium in the hydrogel and the electrode itself. However, the obtained cyclic voltammogram revealed no visible osmium redox peaks on the adjacent electrode. This raises concern because this indicates that the polymer insulating layer was not staying confined to the electrode in which the potential was applied.

Assuming that the reason why the adjacent electrode did not detect osmium was because it somehow got insulated with the 1,2-DAB, the question got raised as to whether or not the 1,2-DAB had to be fully covering the electrode in order to shield it from detecting osmium. After

all, complex containing osmium is a very large molecule, so perhaps full coverage of the electrode was not necessary in this case.

In order to attempt to partially cover the electrode, the potential was swept only one time in both the positive and negative direction to electrodeposit the 1,2-DAB onto the left-most electrode. After the hydrogel application, both the middle and right electrode revealed osmium redox peaks. However, the middle electrode still displayed characteristics of being partially insulated; the cyclic voltammogram obtained from the middle electrode displayed a smaller current response to osmium oxidation and reduction than the right-most electrode. In an attempt to obtain osmium redox cyclic voltammograms of the same size on both electrodes that did not have the potential applied to it, and maintaining zero osmium detection on the electrode that did have the potential applied to it, fast scan cyclic voltammetry was employed.

By applying only "bursts" of voltage to the electrode that was needed to be insulated, minimal 1,2 – DAB would become radicalized and diffusion would be limited due to small amount of time in which the radicals would be formed and the small quantity of radicals formed. This would hopefully result in deposition only on the electrode in which the potential had been applied.

This method proved to be advantageous in keeping the 1,2-DAB contained to the electrode in which the potential was applied. The left electrode, which had the 1,2-DAB coated on it, did not reveal any osmium redox peaks after hydrogel application. The middle and right electrodes both displayed osmium redox peaks after hydrogel application, and the peaks were similar in magnitude. Taking this one step further, and investigating whether the electropolymerized 1,2-DAB displayed any directional diffusional preference, the electrodeposition was changed to the middle electrode. In doing this, the cyclic voltammograms

64

obtained from the right and left electrode after hydrogel application would reveal if the 1,2-DAB that was radicalized at the middle electrode deposited only on the middle electrode, if it deposited on both the outer electrodes, or if it preferentially deposited on only one of the outer electrodes. The result that both the outer electrodes did produce cyclic voltammograms with equal osmium redox peaks indicated that the 1,2-DAB stayed confined to the middle electrode. However, the sensitivity of the electrodes was low. Therefore, it was necessary to investigate whether the electrodes produced small responses naturally, or whether the small responses were due to partial, but equal insulation from the electrodeposition onto the middle electrode.

In order to make sure that both of the electrodes were not being coated by the 1,2 – DAB, and that the sensitivity of these small electrodes was just naturally small, a new set of experiments were carried out using RuHex. By using RuHex, a "before" electrodeposition cyclic voltammogram could be taken as well as an "after" electrodeposition cyclic voltammogram, since RuHex can be rinsed off. Using the same set of parameters as with the previous set of experiments, 1,2 – DAB was electrodeposited onto the middle electrode. The electrode was rinsed and placed back into the RuHex solution. The "after" CV for the left and right electrodes overlap almost perfectly, while the middle electrode no long showed RuHex reduction. This indicates that with the given set of parameters, although the sensitivity is low, no apparent 1,2 – DAB was depositing onto the adjacent electrodes.

In conclusion, we were able to selectively deposit 1,2-DAB onto only one electrode in an array of three electrodes. This significance of this will be discussed in detail in the following chapter.

3.6   ACKNOWLEDGEMENTS

4.0 THE USE OF TRIPLE BAND ARRAY PLATINUM ELECTRODES FOR OXYGEN GENERATION AND GLUCOSE DETECTION UNDER HYPOXIC CONDITIONS

4.1 ABSTRACT

Carbon fiber microelectrodes have been the platform for much of the research involving enxyme-trapping redox hydrogels which allow for the detection of substances in the brain that are not themselves electroactive, such as glucose, choline, and glutamate. Within the scheme of events that takes place in the hydrogel, oxygen is always consumed. Although this does not create a problem when studying most disease states, it does create a problem when studying conditions that are found in hypoxic tissue. To date, there has not been an extensive amount of research on developing electrodes or electrode systems to measure substances, such as glucose, under hypoxic conditions. Herein, we show that using an array band Pt electrode, glucose can be measured under hypoxic conditions. Here, oxygen generation is controlled at one of the electrodes by changing the applied potential from one in which oxygen cannot be generated at (900 mV vs Ag/Agcl) to one at which oxygen can be generated (1200 mV vs Ag/AgCl). When no oxygen is being generated in a nitrogen purged solution, the current response in 3 mM and 6 mM glucose solutions is virtually zero. However, when oxygen is being generated, there is a substantial increase in current (concentration dependant) due to the oxygen playing a role in the

scheme of events within the hydrogel, thus allowing glucose to be measured at an adjacent electrode. In order to ensure that this electrode will be functional in the brain without any interference from ascorbic acid, the electrode was coated with Nafion. Here we show that the response to glucose with the Nafion coating and ascorbic acid in solution is very similar to that in which the electrode was not coated with Nafion and placed in a solution that did not contain ascorbic acid, indicating that application of Nafion did not significantly reduce the detected current and that ascorbic acid did not interfere with the current response associated with glucose detection.

4.2   INTRODUCTION

Electrochemical detection of neurotransmitters and other species in the extracellular space of the brain has been performed by numerous research groups (Cui et al., 2001; Hu et al., 1994; Kulagina et al., 1999; Lowry et al., 1998). Detection methods include using carbon fiber microelectrodes (Garguilo and Michael, 1996; Kulagina et al., 1999) as well as Pt electrodes (Hu and Wilson, 1997; Wang et al., 1997) in conjunction with enzyme trapping redox hydrogels (Cui et al., 2001; Garguilo and Michael, 1996; Ohara et al., 1994).

Enzyme-trapping redox hydrogels are of particular importance in studying the extracellular space of the brain because it allows for species to be detected that are not themselves electroactive (Mitala and Michael, 2006). The hydrogel serves to immobilize the enzymes and mediate the electron transfer between the enzymes, in particular horseradish peroxidase, and the electrode surface. It is important during this process that the enzymes

68

remain in their active form inside the hydrogel (Heller, 1992); inactive enzymes would decrease

the signal and sensitivity of the electrode. Fig 14.
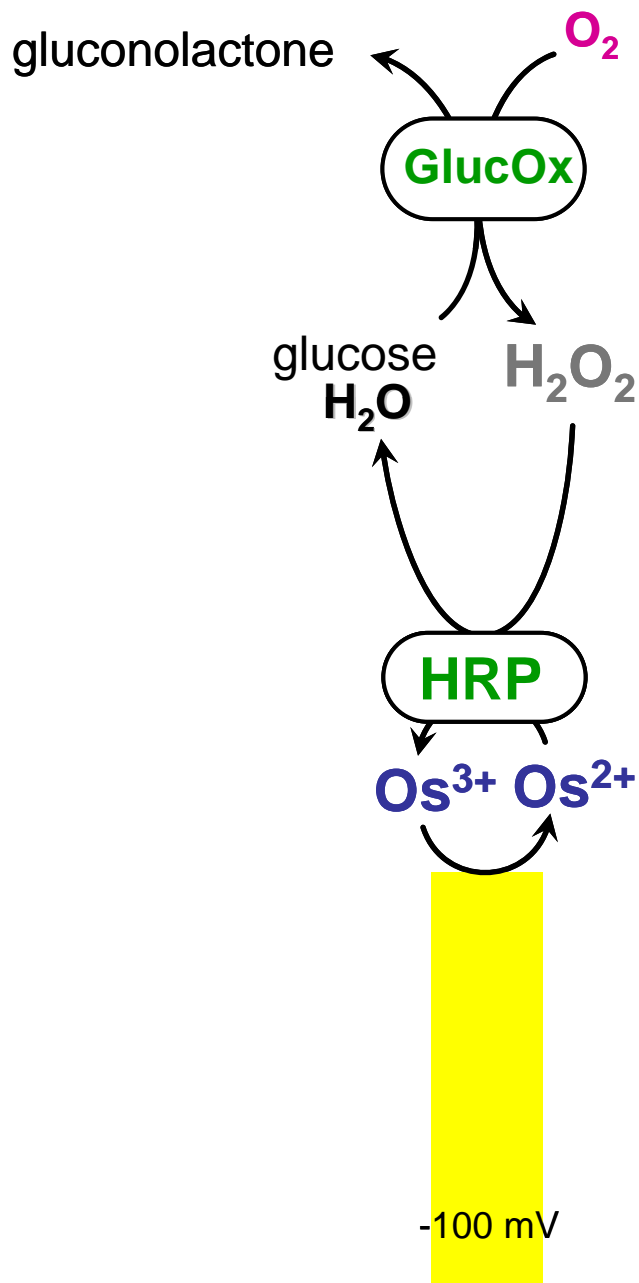
Figure 14: **Typical scheme for the electrochemical detection of glucose with an enzyme sensor. Oxygen is reduced to hydrogen peroxide while glucose is oxidized to gluconolactone via glucose oxidase followed by the reduction of hydrogen peroxide to water when osmium^{2+} is oxidized to osmium^{3+} via horseradish peroxidase. Osmium^{3+} is reduced**

to osmium^{2+} at the electrode surface when the the electrode is held at -100 mV vs Ag/AgCl reference electrode.

One significant point that needs to be made is that the research to date using enzyme-trapping redox hydrogels has required oxygen to be present in order to start the cascade of events; the first being the oxidation of glucose (in our case) to gluconolactone via glucose oxidase while simultaneously reducing oxygen to hydrogen peroxide. There has not been a significant amount of research investigating levels of extracellular substances in the absence oxygen (hypoxic conditions).   Therefore, our strategy is to develop a sensor with an enzyme-trapping redox hydrogel that is capable of detecting extracellular substances in the brain under hypoxic conditions. This is extremely important because there are conditions that result in oxygen deficient tissue; one such condition is traumatic brain injury (Gopinath and Robertson, 1999).

The extracellular substance we are investigating under hypoxic conditions is glucose. Glucose plays many roles inside the body. In mammalians, for instance, it is glucose that provides the energy to maintain proper functioning inside the brain (Siesjo, 1978), and glucose concentrations are also altered in diabetes (Heller, 1999) and traumatic brain injury (Vespa et al., 2005). In order to do this, we designed a three Pt electrodes array in which the outer electrode will generate oxygen in a controlled manner to drive the reactions within the hydrogel of the central electrode, and yet when the generator is turned off, oxygen levels fall to zero, or near zero, thus maintaining the hypoxic environment.   Fig 15.   In order to achieve this, the concentration of the components within the hydrogel had to be optimized as well as the thickness of the hydrogel. Determining the optimal concentration of the components for the hydrogel was based largely on trial and error. In both optimizations, the concentration and thickness used was not considered optimal until at least three different electrodes produced the same or very similar results on three different days.
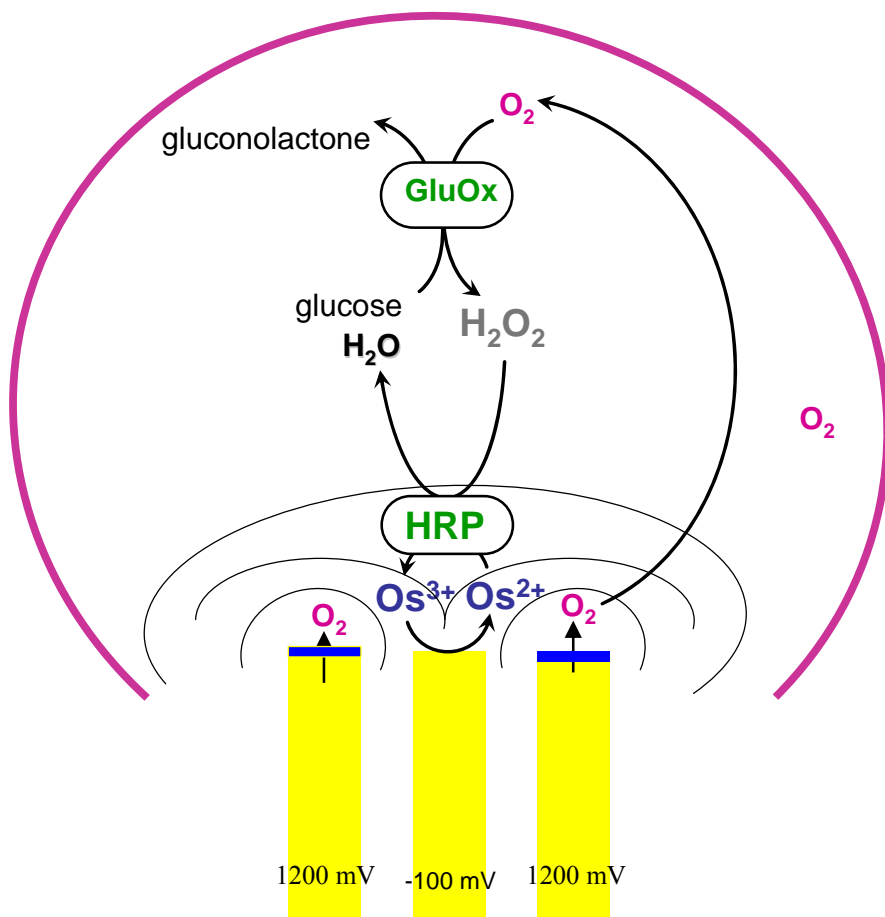
Figure 15: Pt array band design. Since the electrodes are in close proximity to each other, the diffusion layers will overlap. Over time, a local area containing oxygen will develop and oxygen will then be able to start the cascade of events as described in figure 14. An insulating layer, 1,2-DAB, is deposited onto the outer electrodes to prevent osmium[2+] from being oxidized to osmium[3+] on the outer electrode's surface.

73

4.3   MATERIALS AND METHODS

4.3.1   Chemicals and solutions

All reagents were used as received. Horseradish peroxidase (EC 1.11.1.7, type II, HRP), glucose oxidase (type II;   from *Aspergillus niger*), D-(+)-glucose, (+)-sodium-L-ascorbate, and 1,2-diaminobenzene were obtained from Sigma (St. Louis, MO, USA). Nafion, (5 wt % solution in a mixture of lower aliphatic alcohols and water, 1100 equivalent weight diluted to 0.5% with 2-propanol before use), 4-(2-hydroxyethyl)-1-piperazineethanesulfonic acid (HEPES) and HEPES sodium salt were from Aldrich (Milwaukee, WI, USA). Poly(ethylene glycol 400 diglycidyl ether) (PEDGE) was from Polysciences Inc. (Warrington, PA, USA).   1,2-DAB was dissolved in phosphate buffered saline (PBS: 155 mM NaCl, 100 mM phosphate, pH 7.4). Chemicals for and the synthesis of the osmium redox polymer are as reported in Gregg, B.A. and Heller, A. (Gregg and Heller, 1990), and modified as reported in Mitala, J.J. and Michael, A.C. (Mitala and Michael, 2006). Nitrogen gas was received from Valley National Gas (West Mifflin, PA). All solutions were prepared with ultrapure water (NANOPure; Barnstead, Dubuque, IA).

4.3.2 Hydrogel films

The redox polymer (4 mg/mL, 20 uL) and cross-linker (PEDGE, 3 mg/mL, 16 uL) were dissolved in nano-pure DI water (Nanopure, Barstead, Dubuque, IA). HRP (3 mg/mL, 10 uL) and glucose oxidase (2 mg/mL, 10 uL) were dissolved in HEPES buffer (pH 8.00) prepared by the addition of HEPES sodium salt to a 10 mM solution of the acid.

4.3.3 Fabrication of disk electrodes

The disk electrodes were made in-house. The procedure for manufacturing the electrodes is described in detail in Dressman, S.F. and Michael, A.C. (Dressman and Michael, 1995).

4.3.4 Fabrication of array electrodes

Standard 3-in. silicon wafers were used as substrates. The wafer tops were insulated with silicon dioxide. In order to promote adhesion between the silicon and silicon dioxide, a layer of titanium was used between them. These wafers were purchased from Silicon Quest International, Santa Clara, CA, USA. Photoresist and HMDS were deposited onto the wafer by spin coating (CEE 100CB Spinner/Hotplate). The resist was patterned using UV radiation (Karl Suss MA6 Backside Aligner) through a photomask (Penn State, State College, PA, USA) with the electrode pattern. The wafer was baked for one minute on a 100° C hotplate followed by washing away the resist on the exposed areas of the wafer with a resist developing bath. The wafer was baked for ten minutes in a 120° C oven before etching the Ti/Pt by ion milling. The wafers were O_2 plasma cleaned (Technics Plasma Deposition System) before the insulating layer

was applied to remove any remaining photoresist. The wafers were baked on a 200°C hotplate for twenty minutes to ensure that all moisture was removed. The insulating layer, SU8, was applied using a spin plate (Solitec Photoresist Spinner) afterwhich the wafer was soft baked (65° up to 105° C and held there for ten minutes, and then slowly cooled). The insulating layer was patterned using UV radiation (Karl Suss MA56 Contact Aligner) through a second mask. The wafer was soft baked as stated above. The unexposed area on the wafer were rinsed away with developer, rinsed with IPA and dried with nitrogen. Again, the wafers were oxygen plasma cleaned to descum, i.e. get rid of organic matter on the surface, and hard baked in a 120° C oven for a few hours. The electrodes were diced with a Kulicke and Soffa 780-6 Dicing Saw.

4.3.5   Electrical connections to microfabrication array band electrodes

Individual electrode chips were cleaned by sonicating (Branson, Danbury, CT, USA) in acetone (EMD Chemicals, Inc, Gibbstwon, NJ, USA) for fifteen minutes, rinsed with IPA (EMD Chemicals, Inc, Gibbstwon, NJ, USA), and dried with nitrogen. Each chip was glued (5 − Min Epoxy, ITW Devcon, Danvers, MA, USA to a microscope slide (Fisher, Pittsburgh, PA) and oxygen plasma cleaned (Harrick Plasma Cleaner PDC-3XG, Ithaca, NY, USA) for five minutes, in house. Individual copper wires (Goodfellow, England) were placed such that one end rested on a single contact pad. Once all three wires were in place, the wires were epoxied to the slide. With silver paint, connections were made between the contact pad and wire. The electrodes were allowed to dry overnight.

4.3.6 Electrochemical techniques for 1,2-diaminobenzene electrodeposition onto the disk electrode

Cyclic voltammetry (Keithly Instruments, Cleveland, OH, USA), was performed to electrodeposit the 1,2-DAB onto a single electrode in the array. The potential was swept from -0.5 V to 1.0 V and back to -0.5 V vs Ag/AgCl reference electrode in a 3 mM 1,2-DAB solution. This cycle was continued into two successive cyclic voltammograms overlapped.

4.3.7 Electrochemical techniques for 1,2-diaminobenzene electrodeposition onto microfabricated array band microelectrodes

Cyclic voltammetry was performed to electrodeposit the 1,2-DAB onto a single electrode in the array. The potential was swept from -0.5 V to 1.0 V and back to -0.5 V vs Ag/AgCl reference electrode for three minutes at a rate of 300 V/s and a scan interval of 100 ms in a 3 mM 1,2-DAB solution. After the electrodeposition, the electrodes were rinsed to remove any 1,2-DAB solution from the electrode that was electrodeposited onto the electrode. See previous chapter for more details.

4.3.8 Hydrogel application

A 3 μL drop of the hydrogel was placed onto the disk electrode. The electrode was placed in a 37°C oven for one hour.

4.3.9 Electrochemical techniques for glucose detection

Amperometry was performed on an Ensman Instrumentation 400 potentiostat. Before beginning any experiments, the applied potential was swept from 0 to 600 mV and back to 0 mV vs Ag/AgCl reference electrode on the working electrode (reguardless of geometry). This was to confirm the contact or lack of contact between the hydrogel and the working electrode. The working electrode was equilibrated until the current drift was ~1 pA per 60 s.

The current response to various concentrations of glucose for the disk electrode were obtained by placing the electrode in a well-stirred solution of PBS. The amount of PBS used was based on the desired final concentration of glucose. At time t=20 s, glucose was injected into the PBS solution. The response of the electrode to the injection of glucose was monitored for an additional 100 s. Between each experiment, the electrode was rinsed with PBS and re-equilibrated.

4.3.10 Application of nafion to microfabricated array band microelectrodes

A nafion solution was prepared as described above. The electrode, after hydrogel application, was dipped seven times into the nafion solution. Between each dip, the electrode was dried for one minute under a heat gun.

4.3.11 Turning the oxygen generator on and off

The band electrode, with both the hydrogel and Nafion coating on it, was placed in a 0, 3, or 6 mM glucose solution with ascorbic acid. In order to generate oxygen at the outer electrode, the

78

potential on the EI 400 potentiostat was changed manually every two seconds. Oxygen will be generated when the potential is held at 1200 mV and will not be generated when the potential is held at 900 mV.

4.4   RESULTS

4.4.1   Hydrogen peroxide detection with a Pt electrode

In order to confirm that glucose detection is possible with the components of the hydrogel in the ratio presented above, a calibration was performed on a 10 µm disk Pt electrode. This is the only experiment conducted on the disk electrode. Amperometric responses were recorded with a glucose sensor in an air equilibrated solution, i.e. not purged with nitrogen, of PBS. After the addition of an aliquot of glucose solution to the electrochemical cell, a cathodic response was observed. Here the potential of the central electrode was held at +600 mV. With an increase in glucose concentration, there is a linear increase in measured current. The final concentration of glucose administered to the electrochemical cell was 12 mM. This concentration is well above 3 mM, which is the concentration found *in vivo*. Fig 16.

Detection of H2O2 on 10um Pt disk with new ratio

$y = 14.767x$

$R^2 = 0.9932$
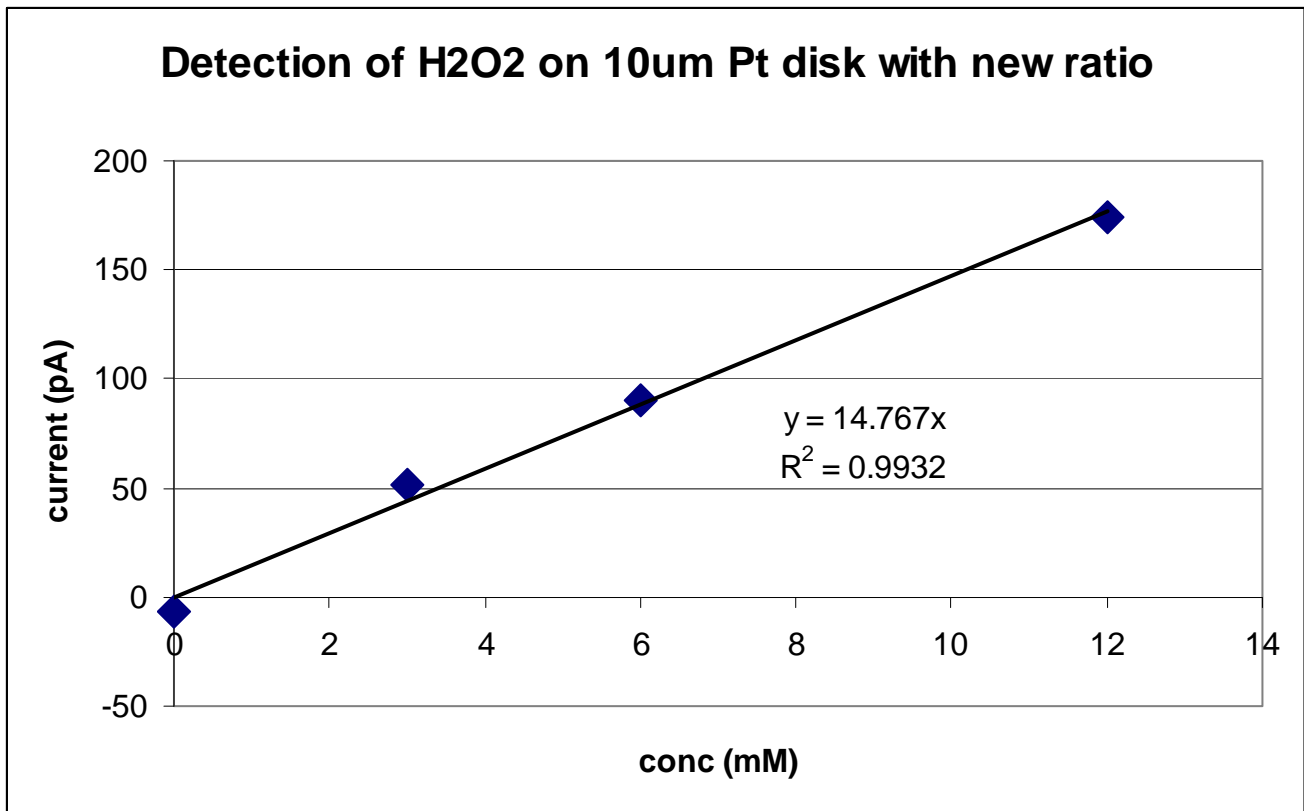
Figure 16: Hydrogen peroxide sensor. With an increase in glucose concentration, the cathodic current response increases.

4.4.2　An operational glucose sensor in the absence of oxygen

4.4.2.1 Confirmation of application of hydrogel

After the electrodeposition of 1,2-DAB, the hydrogel was applied to the electrodes. However, in order for glucose to be detected, the center electrode needs to be free from 1,2-DAB since it acts as a molecular sieve and only allows small molecules such as oxygen to pass through, i.e. osmium is blocked. Therefore, in order to make sure that the center electrode is in contact with osmium, a cyclic voltammogram needs to be obtained in which characteristic oxidation and reduction peaks for osmium are observed. We have shown that it is possible to apply the insulating layer to only the outside electrode. After application of the hydrogel to all three electrodes, the oxygen producing electrode cannot detect osmium because the osmium is blocked due to the presence of the 1,2-DAB, while the center electrode, i.e. glucose electrode, does show evidence of osmium being present. Figs 17a and b.

osmium with 1,2-dab on electrode

osmium with no 1,2-dab on electrode

82
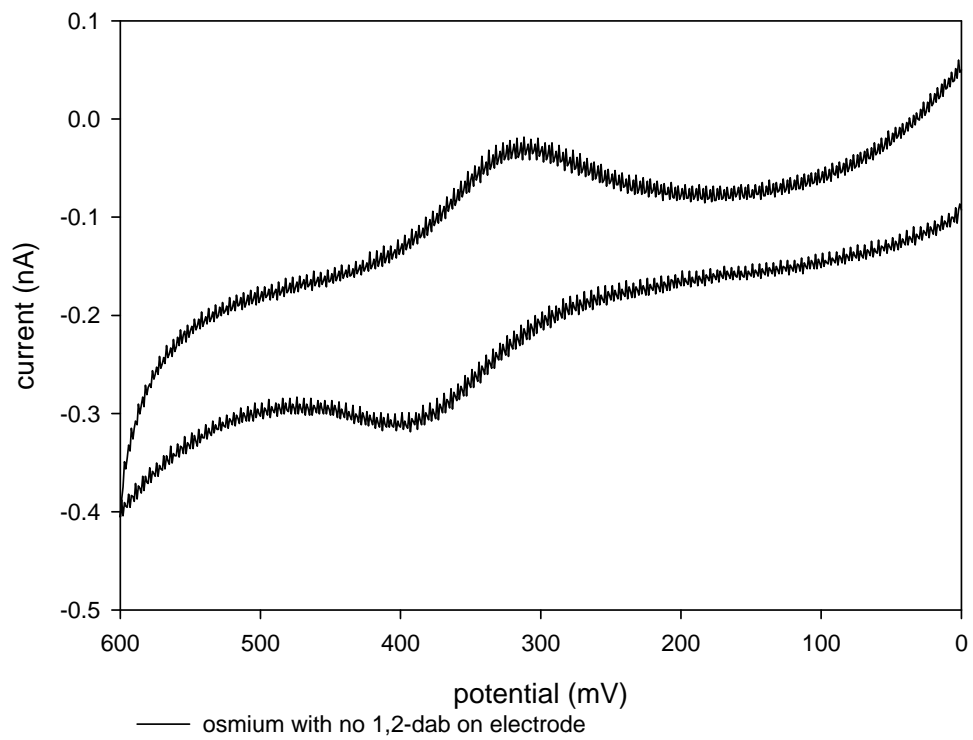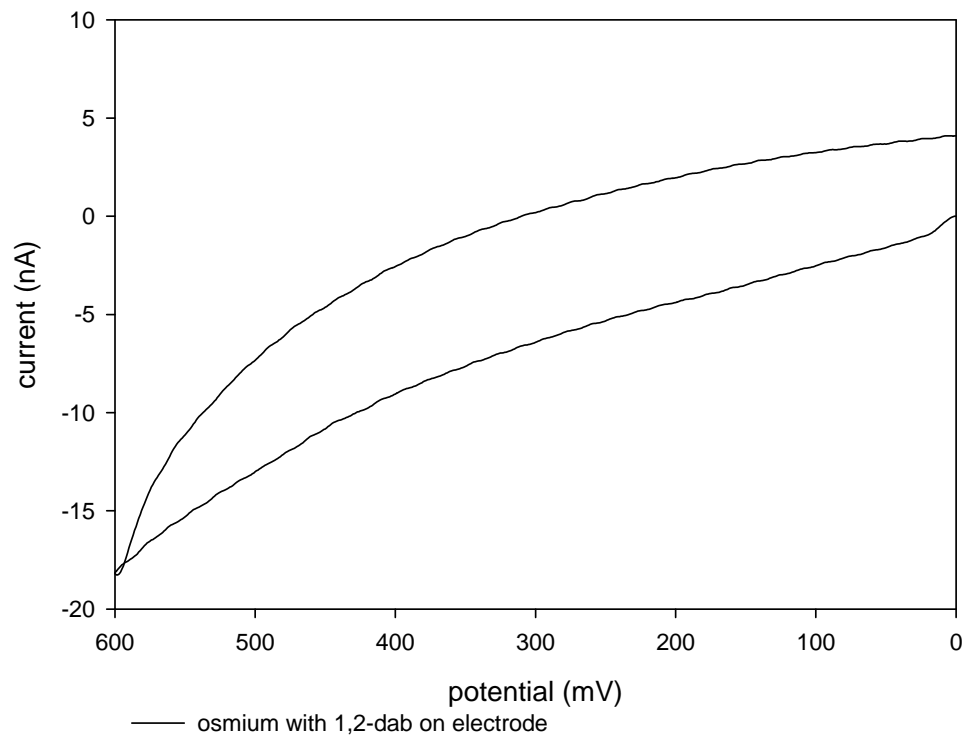
Figure 17: Cyclic voltammograms of two adjacent band electrodes.

a. **Cyclic voltammogram of Pt electrode with 1,2-diaminobenzene electrodeposited on it as well as having the hydrogel applied to it. There is no evidence of osmium detection.**

b. **Cyclic voltammogram of Pt electrode with only the hydrogel applied to it. It is clearly shown that osmium is present based on the oxidation and reduction peaks of osmium.**

4.4.2.2 Confirmation of ascorbic acid present in solution

Since ascorbic acid is an interferent when using enzyme sensors, it is important that our electrodes work in the presence of ascorbic acid. Our electrodes were able to detect glucose in a 300 μM solution of ascorbic acid, and thus we wanted to confirm that the ascorbic acid that was assumed to be in the solution was actually there and able to effect the sensor. Therefore, confirmation of the presence of ascorbic acid in solution is presented in Figure 18. The top trace was taken with an electrode coated with nafion (blocks ascorbic acid from entering the hydrogel) and placed in a solution containing 300 uM ascorbic acid. The bottom trace was taken with a bare electrode in the same solution. Based on the increase in oxidative current with the electrode that is not coated with nafion, it is evident that ascorbic acid is present.
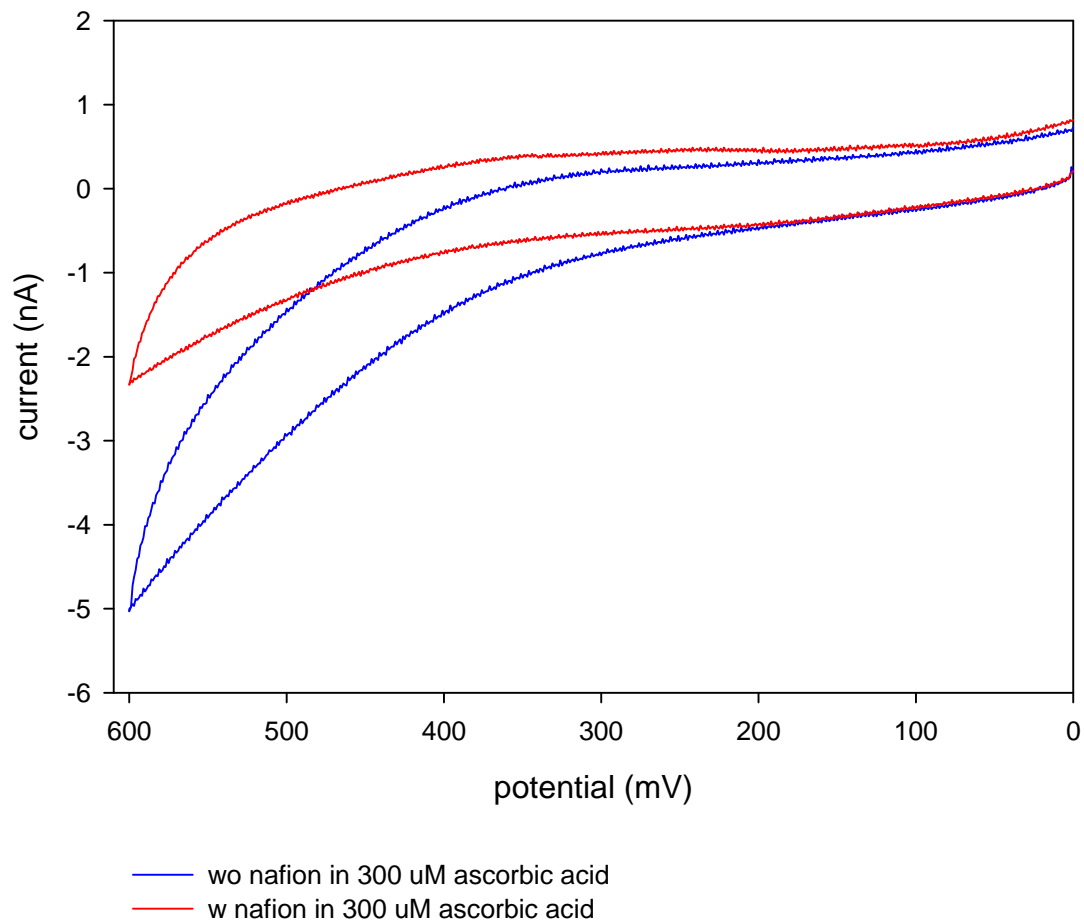
Figure 18: Two traces is a 300 uM solution of ascorbic acid. The top trace is of an electrode that had nafion applied to it. In the bottom trace the electrode did not have nafion applied to it. It is evident that ascorbic acid is present in solution based on the increase in oxidative current when the electrode did not have nafion on it.

4.4.2.3 Glucose detection in ambient and oxygen free cells

The glucose sensors used to generate the data as shown in Figures 19a and b contains the following: 1,2-diaminobenzene on the oxygen generator, hydrogel over entire electrode array, and nafion coating over the entire array. The solution is PBS with 300 μM ascorbic acid. In both cases (ambient and nitrogen purged) when glucose is introduced into the existing solution, the current increases. The current responses are fairly reproducible among the electrodes tested, however, under the nitrogen purged conditions the current response appears to be slightly lower than in ambient conditions. The range of glucose concentrations tested spans from lower than physiological levels to above physiological levels; physiological levels are ~ 3 mM.

a.

b.

87
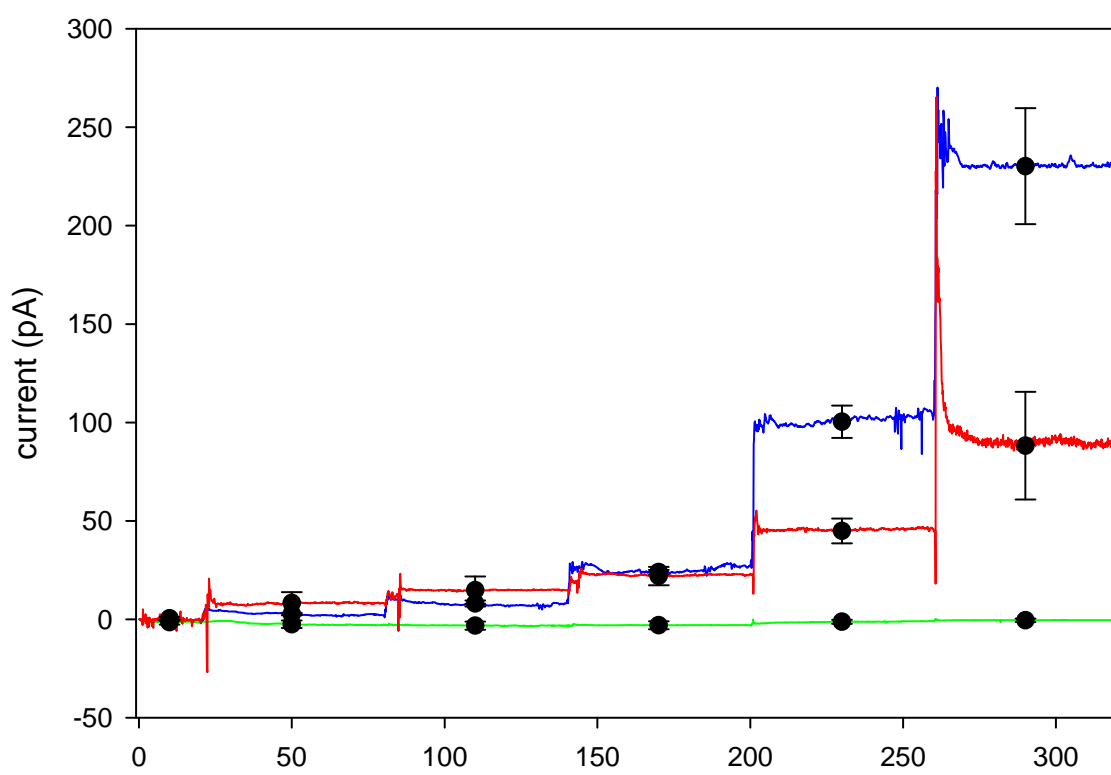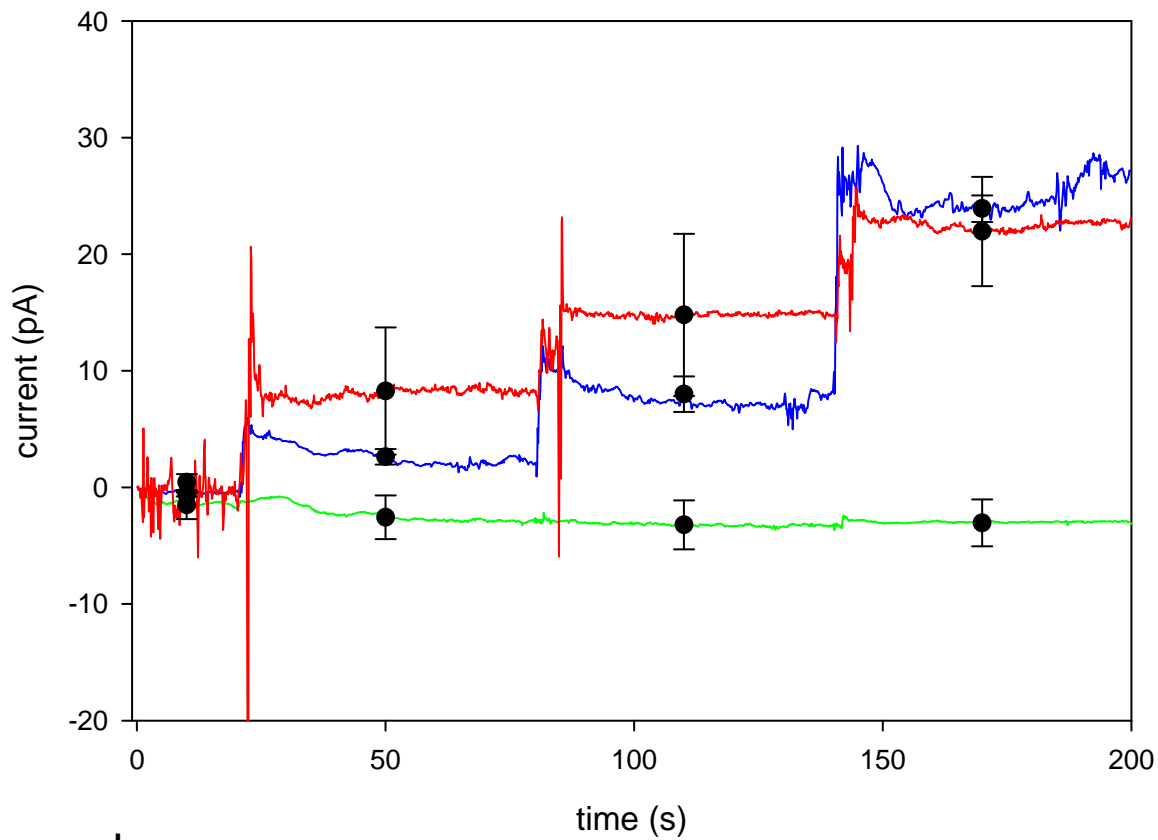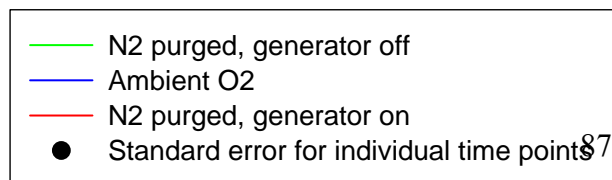
Figure 19: A representative plot of an electrode response to glucose injections.

    a.   Each increase in current response corresponds to an increase in glucose concentration in the beaker: 0 mM; 1 mM; 1.96 mM; 2.88 mM; 3.77 mM; and 4.63 mM glucose.

    b. Blow-up of lower time points.

4.4.2.4 Turning the oxygen generation on and off

The glucose sensors were prepared as discussed above. Here, when the potential applied to the electrode in which oxygen would eventually be generated from was held at +900 mV, a potential too negative to be able to generate oxygen, the current response to glucose was very close to zero. When the potential was flipped to +1200 mV, a potential positive enough to generate oxygen, the current response to glucose increased in a concentration dependant fashion. In the absence of glucose, flipping the potential from one in which oxygen would not be generated to one in which it was, had no effect on the current; the current remained very close to zero. Fig 20.
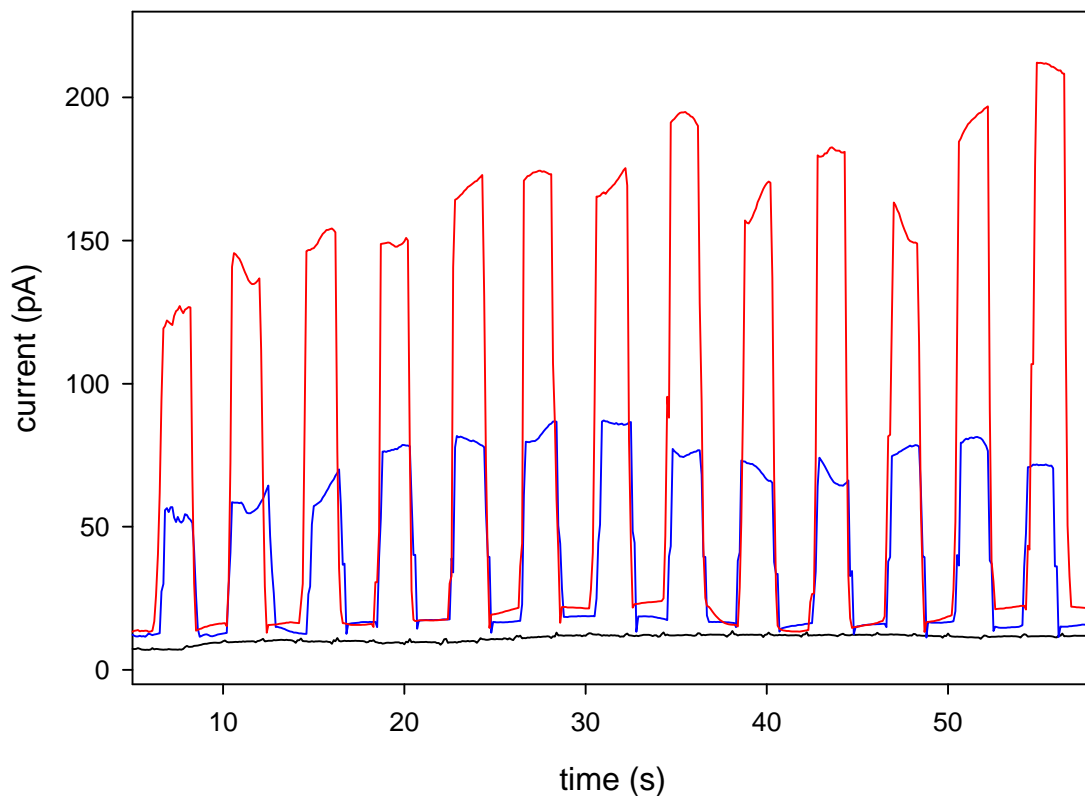
Figure 20: Current responses to glucose as the potential on the generator is flipped between one in which is too low to generate oxygen (900 mV) to one in which oxygen can be generated (1200 mV). The current values reported are absolute values. It is important to note that when no oxygen is being generated the current response returns to baseline levels. The black trace is in the presence of 0 mM glucose, the blue trace is in presence of 3 mM glucose, and the red line is in the presence of 6 mM glucose.

4.5   DISCUSSION

Carbon fiber microelectrodes have been the platform for much of the research involving enzyme-trapping redox hydrogels which allow for the detection of substances in the brain that are not themselves electroactive, such as glucose, choline, and glutamate (Cui et al., 2001; Garguilo and Michael, 1996). As shown in Fig 14, this type of sensor, in particular a glucose sensor that depends on glucose oxidase, requires oxygen to be present. Past research has been able to study glucose levels to better understand diseases, such as diabetes (Heller, A., 1999) and other various conditions (Cui et al., 2001; Linke et al., 1994; Pishko et al., 1991) because oxygen was always present in the local environment.

Understanding the effect of hypoxic conditions on glucose levels is also of great interest (MacCormack and Driedzic, 2006). For instance, how are glucose levels affected after traumatic brain injury; a condition which is known to result in low oxygen levels (Gopinath and Robertson, 1999). In order to gain an understanding of how glucose levels are affected, there needs to be a way to measure glucose when oxygen levels are low.

Figure 15 provides information on how we propose to solve the problem of being able to measure glucose in the absence to oxygen. Here, there are two outer electrodes that will be held at a potential such that oxygen can be generated from water. Because of the close proximity of all of the elecetrodes, the diffusion layers will overlap (Bard and Faulkner, 2001), creating a local environment the does contain oxygen. Oxygen will then be able to start the cascade of reactions as depicted in Figure 14. It is important to note that because the outer two electrodes are held at a positive potential (1200 mV), they will have the ability to oxidize $[Os(bpy)_2(py)Cl]^+$

to $[Os(bpy)_2(py)Cl]^{2+}$. In order to prevent the oxidation of osmium at the outer electrodes, an insulating layer has been electrodeposited onto the surface of the electrode. The insulator used here is 1,2-diaminobenzene. Detailed accounts of why this is the insulator of choice is described in the previos chapter (Mitala and Michael, (in preparation)).

Before performing amperometric experiments on the microfabricated array band Pt electrodes, preliminary experiments were performed on a 10 μm disk Pt electrode. Linear relationships between a carbon fiber microelectrode and glucose concentration has been previously reported (Cui et al., 2001). However, in our hands, using the concentrations and ratios of the components reported in Cui, J., et al. on the Pt electrode did not produce a linear response in relationship to glucose concentration (data not shown). Altering the polymer concentration to 4 mg/mL and altering the glucose oxidase concentration to 2 mg/mL did result in a linear relationship between current response and glucose concentration (Fig 16). The change in these two components can be attributed to the difference in active site area on the electrodes.

One criticism to generating oxygen at an electrode is that now that oxygen has been introduced to the system, one is no longer operating under hypoxic conditions. We set out to show that although oxygen is generated, the generation can be controlled by altering the potential applied to the electrode that is generating the oxygen, and when the potential is not sufficiently positive, current responses return to baseline levels, indicating that no oxygen is present. Figures 16 - 20 show the process that we underwent in order to prove this.

As stated previously, it is necessary for the oxygen generator electrode to be insulated from the rest of the hydrogel so that it does not interfere with any of the other reactions occurring within the hydrogel. It is equally important for the osmium reducing electrode to be free from the insulating layer. Figures 17a and b prove that the insulating layer (1,2-diaminobenzene) can

92

be applied to only the oxygen generating electrode. Figure 16a does not reveal any presence of osmium detection while Figure 17b clearly shows osmium oxidation and reduction peaks.

Interferences from other species that might be present in extracellular fluid must also be accounted for when designing an electrode to eventually be used in vivo. One interference that has been studied in the past is ascorbate. In order to account for any ascorbate that might be present, the electrode was coated with Nafion. Nafion has been shown to reject ascorbate (Cui et al., 2001). In a beaker containing 300 μL ascorbate, the electrode that was coated with Nafion displayed a shallower oxidation current (Fig 18 top trace) than when the electrode had previously been placed in the same solution, only without the Nafion coating (Fig 18 bottom trace). The steeper oxidation current in the bottom trace shows that ascorbate is being oxidized.

Incremental additions of glucose to the PBS and ascorbate solution resulted in incremental current increases in both ambient and nitrogen purged, generator on conditions (Fig 19a and b). The response times to the addition of glucose are virtually immediate. The fast response times can be attributed to the tiny volume of hydrogel applied to the electrode which reduces diffusion time through the hydrogel (Mikeladze et al., 2002).

The different microfabricated electrodes produced results that were reproducible. The current response between ambient and nitrogen purged, generator on conditions agree fairly well. This indicates that the oxygen generation is efficient and can start the cascade of events within the hydrogel. Also, because the current responses are similar, it can be assumed that the oxygen that is being generated is not diffusing in other directions and that most of the oxygen is being used to play a role in the cascade of events.   Since the response times are all instantaneous, once can conclude that the hydrogel volume/thickness is small and diffusion can occur rapidly through the hydrogel.

Although these results indicate that our oxygen generator is indeed efficient at starting the cascade of events, it is important to be able to shut off the oxygen generator in order to prevent producing an environment that is saturated with oxygen, and thus, no longer oxygen deficient. Figure 20 indicates that by flipping the potential from one in which oxygen cannot be generated (900 mV), to one in which it can (1200 mV), allows glucose to be detected. It is imperative that when the generator is turned off the current response returns to baseline levels. Non-baseline currents when no oxygen is being generated would indicate that there is some oxygen lingering around and glucose is still being detected or a little oxygen is somehow still being generated and thus allowing glucose to be detected. Either case would indicate that the system is not efficient.

4.6   ACKNOWLEDGEMENTS

BIBLIOGRAPHY

Abercrombie ED, Keefe KA, DiFrischia DS, Zigmond MJ. Differential effect of stress on in vivo dopamine release in striatum, nucleus accumbens, and medial frontal cortex. J. Neurochem., 1989; 52: 1655-8.

Adams RN. In vivo electrochemical measurements in the CNS. Progress in Neurobiology, 1990; 35: 297-311.

Arrigan DWM. Nanoelectrodes, nanoelectrode arrays and their applications. The Analyst, 2004; 129: 1157-65.

Bard AJ, Faulkner LR. Electrochemical Methods; Fundamentals and Applications, 2 ed. John Wiley & Sons, Inc.: New York, 2001.

Bartley J, Soltau T, Wimborne H, Kim S, Martin-Studdard A, Hess D, Hill W, Waller J, Carroll J. BrdU-positive cells in the neonatal mouse hippocampus following hypoxic-ischemic brain injury. BM.C. Neuroscience, 2005; 6: 15-23.

Bauer R, Brust P, Walter B, Vorwieger G, Bergmann R, Fuchtner F, Steinback J, El-Hallag E, Fritz A, Johannsen B, Zwiener U. Relation between brain tissue pO_2 and dopamine synthesis of basal ganglia - A [18]FDOPA-PET study in newborn piglets. J. Perinatal Medicine, 2000; 28: 54-60.

Benveniste H. Brain microdialysis. Journal of Neurochemistry, 1989; 52: 1667-79.

Benveniste H, Drejer J, Schousbe A, Diemer NH. Elevation of the extracellular concentrations of glutamate and aspartate in rat hippocampus during transiet cerebral ischemia monitored by intracerebral microdialysis. J. Neurochem., 1984; 43: 1369-74.

Benveniste H, Drejer J, Schousbe A, Diemer NH. Regional cerbral glucose phosphorylation and blood flow after insertion of a microdialysis fiber through the dorsal hippocampus in the rat. J. Neurochem., 1987; 49: 729-34.

Blaha CD. Evaluation of stearate-graphite paste electrodes for chronic measurement of extracellular dopamine concentrations in the mammalian brain. Pharmacology

Biochemistryr & Behavior, 1996; 55: 351-364.

Borland LM, Michael AC. Voltammetric study of the control of striatal dopamine release by glutamate. J. Neurochem., 2004; 91: 220-9.

Borland LM, Shi G, Yang H, Michael AC. Voltammetric study of extracelllar dopamine near microdialysis probes acutely implanted in the striatum of the anesthetized rat. J. Neurochem. Methods, 2005; 146: 149-58.

Brannan T,Weinberger J, Knott P, Taff I, Kaufmann H, Togasaki D, Nieves-Rosa J, Maker H. Direct evidence of acute, massive striatal dopamine release in gerbils with unilateral strokes. Stroke, 1987; 18: 108-110.

Bungay PM, Newton-Vinson P, Isele W, Garris PA, Justice JBJ. Microdialysis of dopamine interpreted with quantitative model incorporating probe implantation trauma. J. Neurochem., 2003; 86: 932-46.

Burmeister JJ, Palmer M, Gerhardt GA. L-lactate measures in brain tissue with ceramic-based multisite microelectrodes. Biosensors and Bioelectronics, 2005; 20: 1772-9.

Butcher SP, Fairbrother IS, Kelly JS, Arbuthnott GW. Amphetamine-induced dopamine release in the rat striatum: an in vivo microdialysis study. Journal of Neurochemistry, 1988; 50: 346–355.

Carlsson A, Waters N, Carlsson ML. Neurotransmitter interactions in schizophrenia - therapeutic implications. Biol. Psychiatry, 1999; 46: 1388-95.

Carlsson M, Carlsson A. Interactions between glutamatergic and monoamergic systems within the basal ganglia - implications for schizophrenia and Parkinson's disease. TINS, 1990; 13: 272-6.

Caston SL, McCarley RL. Characteristics of nanoscopic Au band electrodes. J. Electroanal. Chem., 2002; 529: 124-34.

Choi DW, Koh J, Peters S. Pharmacology of glutamate neurotoxicity in cortical cell culture: Attenuation by NMDA antagonists. J. Neurosci., 1988; 8: 185-196.

Choi DW, Rothman SM. The role of glutamate neurotoxicity in hypoxic-ischemic neuronal death. Ann. Rev. Neurosci., 1990; 13: 171-182.

Clapp-Lilly KL, Roberts RC, Duffy LK, Irons KP, Hu Y, Drew KL. An ultrastructural analysis of tissue surrounding a microdialysis probe. J. Neurochem. Methods, 1999; 90: 129-42.

Cookson, M. R. (2005) The biochemistry of Parkinson's disease. *Ann. Rev. Biochem.,* **74,** 29-52.

Cooper JR, Bloom FE, Roth RH. The biochemical basis of neuropharmacology, 7th Edition. 1996; Oxford University Press; Oxford. pp231-234.

Cui J, Kulagina NV, Michael AC. Pharmacological evidence for the selectivity of in vivo signals obtained with enzyme-based electrochemical sensors. J. Neurosci. Methods, 2001; 104: 183-9.

Desce JM, Godeheu G, Galli T, Artaud F, Cheramy A, Glowinski J. L-glutamate-evoked release of dopamine from synaptosomes of the rat striatum: involvement of AMPA and N-methyl-D-aspartate receptors. Neuroscience, 1992; 47: 333-339.

DiChiara G, Tanda G, Carboni E. Estimation of in-vivo neurotransmitter release by brain microdialysis: The issue of validity. Behav. Pharmacol., 1996; 7: 640-57.

Dressman SF, Michael AC. On-line electrochemical detection or supercritical fluid chromatography. Anal. Chem., 1995; 67: 1339-45.

Dressman SF, Peters JL, Michael AC. Carbon fiber microelectrodes with multiple sensing elements for in vivo voltammetry. J. Neuroscience Methods, 2002; 119: 75-81.

Elsworth JD, Roth RH. Dopamine synthesis, uptake, metaboloism, and receptors: relevance to gene therapy of Parkinson's Disease. Experimental Neurology, 1997; 144: 4-9.

Ewing Ag, Bigelo JC, Wightman RM. Direct in vivo monitoring of dopamine released from two striatal compartments. Science, 1983; 221: 169-170.

Fillenz M, Lowry JP. The relation between local cerebral blood flow and extracellular glucose concentration in rat striatum. Experimental Physiology. 1998; 83: 233-238.

Fonnum FJ. Glutamate: a neurotransmitter in mammalian brain. J. Neurochem., 1984; 42: 1-11.

Foster A, Gill R, Woodruff GN. Neuroprotective effects of MK-801 in vivo: Selectivity and evidence for delayed degeneration mediated by NMDA receptor activation. J. Neurosci., 1988; 8: 4745-4754.

Garguilo MG, Michael AC. Amperometric microsensors for monitoring choline in the extracellular fluid of brain. J. Neurosci. Methods, 1996; 70: 73-82.

Garris PA, Collins LB, Jones SR, Wighman RM. Evoked extracellular dopamine in vivo in the medial prefrontal cortex. Journal of Neurochemistry, 1993; 61: 637-647.

Garris. PA, Wightman RM. Different kinetics govern dopaminergic transmission in the amygdala, prefrontal cortex and striatum: an in vivo voltammetric study. Journal of Neuroscience, 1994, 1994; 14: 442-450.

Gibson GE, Huang HM. Animal models of brain hypoxia. From: Neuromethods, Vol. 22, Animal models of neurological disease, II. ed. A Boulton, G Baker, and R Butterowrth, The Humana Press Inc, 1992; 51-93.

Giorguieff MF, Kemel ML, Glowinski J. Presynaptic effect of L-glutamic acid on the release of dopamine in rat striatal slices. Neuroscience Letters, 1977; 6: 73-77.

Gopinath SP, Robertson CS, editors. In Traumatic Brain Injury. Thieme Medical Publishers: New York City, 1999.

Grace AA. Phasic versus tonic dopamine release and the modulation of dopamine system responsivity: A hypothesis for the etiology of schizophrenia. Neuroscience, 1991; 41: 1-24.

Gregg BA, Heller A. Cross-linked redox gels containing glucose oxidase for amperometric biosensor applications. Anal. Chem., 1990; 62: 258-63.

Groothuis, DR, Ward S, Schlageter KE, Itskovich AC, Schwerin SC, Allen CV, Dills C, Levy RM. Changes in blood-brain barrier permeability associated with insertion of brain cannulas and microdialysis probes. Brain Res. 1998; 803: 218-230.

Heineman WR, Wieck HJ, Yacynych AM. Polymer film chemically modified eelctrode as a potentiometric sensor. Anal. Chem., 1980; 52: 345-6.

Heller A. Electrical connection of enzyme redox centers to electrodes. J. Phys. Chem., 1992; 96: 3579-87.

Heller A. Implanted electrochemical glucose sensors for the management of diabetes. Annu. Rev. Biomed. Enng., 1999; 01: 153-75.

Hopwood SE, Parkin MC, Bezzina EL, Boutelle MG, Strong AJ. Transient changes in cortical glucose and lactate levels associated with peri-infarct depolarisations, studied with rapid-sampling microdialysis. Journal of Cereb. Blood Flow and Metabolism, 2005; 25: 391-401.

Hu Y, Mitchell K, Albahadily F, Michaelis E, Wilson G. Direct measurement of glutamate release in the brain using dual enzyme-basedelectrochemicala sensor. Brain Res., 1994; 659: 117-25.

Hu Y, Wilson GS. Rapid changes in local extracellular rat brain glucose observed with an in vivo glucose sensor. J. Neurochem., 1997; 68: 1745-52.

Iwasaki Y, Morita M. Electrochemical measurements withi interdigitated array microelectrodes. Current Separations, 1995; 14: 1-8.

Jasper MS, McDermott P, Gann DS, Engeland WC. Measurement of blood flow to the adrenal capsule, cortex and medulla in dogs after hemorrhage by fluorescent microshperes. J. Auton. Nerv. Syst., 1990; 30: 159-68.

Jones SR, Gainetdinov RR, Caron MG. Application of microdialysis and voltammetry to assess dopamine functions in genetically altered mice: correlation with locomotor activity. Psychopharmacology, 1999; 147: 30-2.

Jones SR, Gainetdinov RR, Jaber M, Giros B, Wightman RM, Caron MG. Profound neuronal plasticity in response to inactivation of the dopamine transporter. Proc. Natl. Acad. Sci. USA, 1998; 95: 4029-4034.

Jung MC, Munro S, Shi G, Michael AC, Weber SG. Use of tris(2,2'-bipyridine)osmium as a photoluminescence-following electron-transfer (PFET) reagent for postcolumn detection in capillary high performance liquid chromatography. Anal. Chem., 2006a; 78: 1761-8.

Jung MC, Shi G, Borland LM, Michael AC, Weber SG. Simultaneous determination of biogenic monoamines in rat brain dialsates using capillary high-performance liquid chromatography with photoluminescence-following electron-transfer. Anal. Chem., 2006b; 78: 1755-60.

Kaakkola A, Tuomainen P, Wurtman RJ, Mannisto PT. Effects of systemic carbidopa synthesis in a rat hypothalamus and striatum. J. Neural Transm., 1992; 4: 143-54.

Kashii S, Takashi M, Mandai M, Shimizu H, Honda Y, Sasa M, Ujihara H, Tamura Y, Yokota T, Akaike A. Protective action of dopamine against glutamate neurotoxicity in the retina. Investigative Ophthalmology & Visual Science, 1994; 35: 685-695.

Kennedy RT, Jones SR, Wightman RM. Simultaneous measurement of oxygen and dopamine: Coupling of oxygen consumption and neurotransmission. Neuroscience, 1992; 47: 603-612.

Koob GF, Bloom FE. Cellular and moldecular mechanisms of drug dependance. Science, 1988; 242: 715-23.

Kulagina NV, Michael AC. Monitoring hydrogen peroxide in the extracellular space of the brain with amperometric microsensors. Anal. Chem., 2003; 75: 4875-4881.

Kulagina NV, Shankar L, Michael AC. Monitoring glutamate and ascorbate in the extracellular space of brain tissue with electrochemical microsensors. Anal. Chem., 1999; 71: 5093-100.

Kulagina NV, Zigmond MJ, Michael AC. Glutamate regulates the spontaneous and evoked release of dopamine in the rat striatum. Neuroscience, 2001; 102: 121-8.

Kuo MF, Wu RM, Wang HS, Lin SM. CPP antagonizes hypoxia-induced changes in dopamine metabolism in the striatum of newborn rat. Neuroscience Research, 1999; 35: 347-350.

Kietzmann T, Krones-Hertzig A, Jungermann K. Signaling cross-talk between hypoxia and

glucose via hypoxia-inducible factor 1 and glucose response elements. Biochemical Pharmacology. 2002; 64: 903-911.

Lanyon YH, Arrigan DWM. Recessed nanoband electrodes fabricated by focused ion beam milling. Sensors and Actuators B, 2007; 121: 341-7.

Leviel V. The reverse transport of DA, what physiological significance? Neurochem. Int., 2001; 38: 83-106.

Linke B, Kerner W, Kiwit M, Pishko M, Heller A. Amperometric biosensor for in vivo glucose sensing based on glucose oxidase immobilized in a redox hydrogel. Biosensors and Bioelectronics, 1994; 9: 151-8.

Lowry JP, Ryan MR, O'Neill RD. Behaviourally induced chances in extracellular levels of brain glutamate monitored at 1 s resolution with an implanted biosensor. Anal. Commun., 1998; 35: 87-9.

Lu Y, Peters JL, Michael AC. Direct comparison of the response of voltammetry and microdialysis to electrically evoked release of striatal dopamine. J. Neurochem., 1998; 70: 584-93.

MacCormack TJ, Driedzic WR. The impact of hypoxia on invivo glucose uptake in a hypoglycemic fish, *Myoxocephalus scorpius*. Am. J. Physiol. Regul. Integr. Comp. Physiol., 2006; 292: 1033-42.

Martinez-Leon NC. Psychopathology of attention deficit/hyperactivity disorder (AD/HD). International Journal of Clinical and Health Psychology,2006; 6: 379-399.

Mikeladze E, Schulte A, Mosbach M, Blochl A, E. C, Solomonia R, Schumann W. Redox hydrogel-based bienzyme microelectrodes for amperometric monitoring of L-glutamate. Electroanalysis, 2002; 14: 393-9.

Miller HH, Shore PA. Effects of amphetamine and amfonelic acid on the disposition of striatal newly synthesized dopamine. Eur J Pharmacol, 1982; 78:33-44.

Mitala CM, Michael AC. (in preparation).

Mitala CM, Wang Y, Borland LM, Jung M, Shand S, Watkins S, Weber SG, Michael AC. Impact of microdialysis probes on vasculature and dopamine in the rat striatum: a combined fluorescence and voltammetric study. J. Neurosci. Methods, 2008; submitted.

Mitala JJ, Michael AC. Improving the performance of electrochemical microsensors based on enzymes entrapped in a redox hydrogel. Analytica Chimica Acta, 2006; 556: 326-32.

Moghaddam BJ. Stress preferentially increases extraneuronal levels of excitatory amino acids in the prefrontal cortex: comparison to hippocampus and basal ganglia. J. Neurochem., 1993, 60: 1650-1657.

Molecular Probes. Working with Fluorspheres Fluorescent Microspheres. http://probes.invitrogen.com/media.pis/mp05001.pdf, 2004.

Morris RB, Franta DJ, White HS. Electrochemistry at Pt band electrodes of width approaching molecular dimensions. Breakdown of transport equations at very small electrodes. J. Phys. Chem., 1987; 91: 3559-64.

Nagale MP, Fritsch I. Individually addressable, submicrometer band electrode arrays. 2. Electrochemical characterization. Anal. Chem., 1998; 70: 2908-13.

Neher E. Vesicle pools and Ca2+ microdomains: new tools for understanding their roles in neurotransmitter release. Neuron, 1998; 20: 389-399.

Ohara TJ, Rajagopalan R, Heller A. "Wired" enzyme electrodes for amerometric determination of glucose or lactate in the presence of interfering substances. Anal. Chem., 1994; 66: 2451-7.

Olney JW. Neurotoxicity of excitatory amino acids. In Kainic acid as a tool in neurobiology, ed. EG McGeer, JW Olney, PL McGeer, 1978; New York: Raven: 95-171.

Olney JW, Sharpe LG. Brain lesions in an infant rhesus monkey treated with monosodium glutamate. Science, 1969; 166: 386-388.

Orset C, Parrot S, Sauvinet V, Cottet-Emard JM, Pequignot JM, Denoroy L. NMDA receptors inhibit the mild hypoxia-induced dopamine efflux in the rat striatum. Synpase, 2006; 59: 458-461.

Pellegrino LJ, Pellegrino As, Cushman AJ, editors. A stereotaxic atlas of the rat brain. 2nd edition. Plenum Press: New York, 1979.

Peters JL, Michael AC. Modelling voltammetry and microdialysis of striatal extracellular dopamine: The impact of daopamine uptake on extraction and recovery ratios. J. Neurochem., 1998; 70: 594-603.

Peters JL, Miner LH, Michael AC, Sesack SR. Ultrastructure at carbon fiber microelectrode implantation sites after acute voltammetric measurements in the striatum of anesthetized rats. J. Neurosci. Methods, 2004; 137: 9-23.

Pishko MV, Michael AC, Heller A. Amperometric glucose microelectrodes prepared through immobilization of glucose oxidase in redox hydrogels. Anal. Chem., 1991; 63: 2268-72.

Qian J, Wu Y, Michael AC. An integrated decoupler for capillary electrophoresis with electrochemical detection: application to analysis of brain microdialysate. Anal. Chem., 1999; 71: 4486-92.

Ract C, Vigue B, Bodjarian N, Mazoit JX, Samii K, Tadie M. Comparison of dopamine and norepinephrine after traumatic brain injury and hypoxic-hypotensive insult. Journal of Neurotrauma, 2001; 18: 1247-1254.

Raiteri M, Cerrito F, Cervoni AM, Levi G. Dopamine can be released by two mechanisms differentially affected by the dopamine transport inhibitor nomifensine. The Journal of Pharmacology and Experimental Therapeutics, 1979; 208: 195-202.

Rothman SM. Synaptic release of excitatory amino acid neurotransmitter mediates anoxic neuronal death. J. Neurosci., 1984; 4: 1884-1891.

Sabeti J, Adams CE, Burmeister J, Gerhardt GA, Zahniser NR. Kinetic analysis of striatal cleareance of exogenous dopamine recorded by chronoamperometry in freely-moving rats. Journal of Neuroscience Methods, 2002; 121: 41-52.

Sandison ME, Anicet N, Glidle A, Cooper JM. Optimization of the geometry and porosity of microelectrode arrays for sensor design. Anal. Chem., 2002; 74: 5717-25.

Sasso SV, Pierce RJ, Walla R, Yacynych AM. Electropolymerized 1,2-diaminobenzene as a means to prevent interferences and fouling and to stabilize immobilized enzyme in electrochemical biosensors. Anal. Chem., 1990; 62: 1111-7.

Siesjo BK. Brain Energy Metabolism. WIley: New York, 1978.

Smith AD, Justice JBJ. The effect of inhibition of synthesis, release, metabolism and uptake on the microdialysis extraction fraction of dopamine. J. Neurosci. Methods, 1994; 54: 75-82.

Smith AD, Olson RJ, Justice, Jr. JB. Quantitative microdialysis of dopamine in the striatum: effect of circadian variation. Journal of Neuroscience Methods, 1992; 44: 33-41.

Stefano GB, Catapane E, Aiello E. Dopaminergic agents: influence on serotonin in the molluscan nervous system. Science, 1976; 194: 539-41.

Takagi N, Tsuru H, Yamamura M, Takeo S. Changes in striatal dopamine metabolism after microshpere embolism in rats. Stroke, 1995; 26: 1101-1106.

Tang A., Bungay PM, Gonzales, RA. Characterization of probe and tissue factors that influence interpretation of quantitative microdialysis experiments for dopamine. J. Neurosci. Meth. 2003; 126: 1-11.

Tossman U, Erikson S, Delin A, Hagenfeldt L, Law D, Ungerstedt U. Brain amino acids measured by intracerebral dialysis in portacaval shunted rats. J. Neurochem., 1983; 41: 1046-51.

Van Oosterhout MFM, Prinzen FW, Sakurada S, Glenny RW, Hales JRS. Fluorescent

microspheres are superior to radioactive microspheres in chronic blood flow measurements. Am. J. Physiol. Heart Circ. Physiol., 1998; 275: 110-5.

Venton BJ, Seipel AT, Phillips PEM, Wetsel WC, Gitler D., Greengard P, Augustine GJ, Wightman RM. Cocaine increases dopamine release by mobilization of synapsin-dependent reserve pool. J. Neurosci. 2006; 26: 3206-3209.

Vespa P, Bergsneider M, MCArthur D, Wu HM, Huang SC, Alger J, Glenn T, Hovda D. Intensive insulin therapy is assiciated with reduced extracellular glucose and increased oxygen extraction fraction after severe traumatic brain injury. J. Cerebral Blood Flow & Metabolism, 2005; 25: S60.

Wang J, Pamidi PVA, Cepria G, Basak S, Rajeshwar K. Overoxidized poly{pyrrole-co-[3-(pyrrol-1-yl)-propanesulfonate]}-coated platinum electrodes for selective detection of catecholamine neurotransmitters. The Analyst, 1997; 122: 981-4.

Watanabe S, Fusa K, Takada K, Aono Y, Saigusa T, Koshikawa N, Cools AR. Effects of alpha-methyl-p-tyrosine on extracellular dopamine levels in the nucleus accumbens and the dorsal striatum of freely moving rats. Journal of Oral Science, 2005; 47: 185-90.

Westerink BHC, deVries JB. Characterization of in vivo dopamine release as determined by brain microdialysis after acute and subchronic implantations: methodological aspects. J. Neurochem., 1988; 51: 683-7.

Westerink BHC, Hofsteede RM, Tuntler J, DeVries JB. Use of calcium antagonism for the characterization of drug-evoked dopamine release from the brain of conscious rats determined by microdialysis. J. Neurochem., 1989; 52: 722-9.

Wightman RM. Microvoltammetric electrodes. Anal. Chem., 1981; 53: 1125A-1134A.

Wightman RM, Zimmerman JB. Control of dopamine extracellular concentration in rat striatum by impulse flow and uptake. Brain Res. Rev., 1990; 15: 135-144.

Wu H-Q, Rassoulpour A, Schwarcz R. Kynurenic acid leads, dopamine follows: A new case of volume transmission in the brain? . J. Neural Transm., 2007; 114: 33-41.

Wu Q, Reith MEA, Wightman RM, Kawagoe KT, Garris PA. Determination of release and uptake parameters from electrically evoked dopamine dynamics measured by real-time voltammetry. Journal of Neuroscience Methods, 2001; 112: 119-133.

Yang H, Peters JL, Allen C, Chern SS, Coalson RD, Michael AC. A theoretical description of microdialysis with mass transport coupled to chemical events. Anal. Chem., 2000; 72: 2042-9.

Yang H, Peters JL, Michael AC. Coupled effects of mass transfer and uptake kinetics on in vivo microdialysis of dopamine. J. Neurochem., 1998; 71: 684-92.

Yang X, Zhang G. Diffusion-controlled redox cycling at nanoscale interdigitated electrodes. Excerpt from the Proceedings of the COMSOL Multiphysics User's Conference 2005 Boston, 2005.

Zhou F, Shu X, Castellani RJ, Stimmelmayr R, Perry G, Smith MA, Drew KL. Hibernation, a model of neuroprotection. American Journal of Pathology, 2001; 158: 2145-51.

Zimmerman JB and Wightman RM. Simultaneous electrochemical measurements of oxygen and dopamine in vivo. Anal. Chem., 1991; 63, 24-28.